Manuscript for *SAJES*

# Sediment provenance of Triassic and Jurassic sandstones in central Mexico during activity of the Nazas volcanic arc

Marc Wengler[1,2,*], José Rafael Barboza-Gudiño[3], Tonny B. Thomsen[4], Guido Meinhold[1,5]

[1] Geowissenschaftliches Zentrum der Universität Göttingen, Abteilung Sedimentologie/Umweltgeologie, Goldschmidtstraβe 3, D-37077 Göttingen, Germany

[2] Alfred Wegener Institute for Polar and Marine Research, Am Alten Hafen 26, D-27568 Bremerhaven, Germany

[3] Universidad Autónoma de San Luis Potosí, Instituto de Geología, Manuel Nava No. 5, Zona Universitaria, 78240, San Luis Potosí, México

[4] Geological Survey of Denmark and Greenland (GEUS), Øster Voldgade 10, DK-1350 Copenhagen K, Denmark

[5]School of Geography, Geology and the Environment, Keele University, Keele, Staffordshire ST5 5BG, UK

***** Corresponding author. Tel.: +52 444 8171038.
*E-mail address:* rbarboza@uaslp.mx (R. Barboza)

**Abstract**

We have investigated the provenance of Late Triassic and Jurassic siliciclastic sediments (Zacatecas, Nazas and La Joya formations) in the Mesa Central region (areas of La Ballena, Charcas and Real de Catorce) in central Mexico. The sediments were deposited during activity of the Nazas volcanic arc at the western margin of Pangaea. Provenance characteristics are essential for reconstructing the palaeotectonic setting of the region. Overall, 26 sediment samples and 3 volcanic rock samples from the Nazas volcanic arc were analyzed. The latter are potential source lithologies. Petrographic analysis reveals that the

analyzed sediments are mainly composed of monocrystalline quartz, polycrystalline quartz (chert and composite quartz), feldspar, and rock fragments of mainly volcanic origin. Th/Sc vs. Zr/Sc values illustrate low sediment recycling in the source area(s). For the majority of the analyzed samples low Cr and Ni values exclude input from a mafic/ultramafic (ophiolitic) source. The majority of the translucent heavy minerals (Pxn, Amp, Ep, Spn, Grt, Chl, Tur, Ant, Rt) are scarce in almost all samples. The most abundant translucent heavy minerals occurring in the samples are apatite and zircon. Apatite grains decrease from the southeast (La Ballena) towards the northeast (Real de Catorce) either indicating stronger weathering conditions in the area of Real de Catorce or a source area that delivered detritus exclusively for the zone of Real de Catorce. Sediments of the Zacatecas Formation illustrate maximum depositional ages ranging from Norian (Late Triassic) to the Hettangian/Sinemurian boundary (Early Jurassic). Detrital zircon U–Pb ages suggest that they received detritus from the Amazonian craton (~1780–1300 Ma), the Oaxaquia microcontinent (~1290–900 Ma), the Maya (Yucatan–Chiapas), Oaxaquia, Coahuila and possible Chortis, and Florida blocks (~720–450 Ma) and the Permian–Triassic magmatic arc (~300–240 Ma). The Acatlán Complex and the Maya (Yucatan–Chiapas) block are likely source areas for ~445–310 Ma-old zircon grains. The source of the ~240–200 Ma-old detrital zircons are likely magmatic rocks related to the early disassambly of western Pangaea. Detrital zircons from sediments of La Joya Formation provide maximum depositional ages from the Pliensbachian (Early Jurassic) to Oxfordian (Late Jurassic). The most probably source areas are the Oaxaquia microcontinent (~1290–900 Ma), and the Maya (Yucatan–Chiapas), and Coahuila blocks (~720–450 Ma). Zircon ages ranging from ~200–150 Ma are indicative of detritus from the Nazas volcanic arc, which explains the presence of the volcanic fragments in La Joya Formation deposits.

*Keywords:* Sediment provenance; Heavy mineral analysis; U–Pb zircon geochronology; Mesozoic; Nazas arc; NE-Mexico

## 1. Introduction

This study is part of a project that aims to reconstruct the palaeotectonic and palaeogeographic situation in central and northeastern Mexico during the Mesozoic. Furthermore, it focuses on identifying similarities and differences among the study areas of La Ballena, Charcas and Real de Catorce (Figs. 1, 2) in central Mexico. A provenance

analysis of Triassic and Jurassic siliciclastic sediments was carried out to contribute to the understanding of transport directions and depositional areas. So far, only a few studies have been published presenting provenance sensitive data from this area. For example, Rubio-Cisneros and Lawton (2011) presented zircon U–Pb dates of continental redbeds at Valle de Huizachal, which is located ~260 km to the ENE of our northeasternmost study area (Real de Catorce, located in the Sierra de Catorce range) (Fig. 2).

Twenty-nine samples (26 sedimentary and 3 volcanic rocks) in the study areas of La Ballena, Charcas and Real de Catorce in the Mesa Central region were collected for follow-up investigations. The Triassic and Jurassic stratigraphic succession of the selected study areas can be described as diverse because of the complex evolution of the Gulf of Mexico province and the western Pacific Mexico province (Goldhammer, 1999, Martini and Ortega-Gutierrez, 2016). Triassic rocks assigned to the Zacatecas Formation underlie volcanic rocks attributed to a volcanic arc (Nazas arc) or volcanic province (sensu Martini and Ortega-Gutierrez) that was active for a period of 40 Ma during the Jurassic (Barboza-Gudiño et al., 2008). Jurassic redbeds including conglomeratic rocks as well as siltstones and sandstones are interlayered with (Lower Jurassic La Boca Formation) or rest also unconformably (Middle-Jurassic La Joya Formation) on volcanic rocks of the Nazas arc (Fig. 3). However, complete and undisturbed sections without fault zones and other disturbing factors (e.g., weathering) influencing the stratigraphy are nowhere present. Therefore, the assignment of rock samples based on field observations to Triassic or Jurassic geological formations is anything but straightforward and needs to be confirmed by further investigations (e.g., petrography, geochemistry, heavy mineral analysis, and detrital zircon U–Pb geochronology). The characterization and description of rock samples are necessary to compile and correlate stratigraphic profiles of each study area. The identification of the source area is of great importance for the reconstruction of transport directions and depositional regimes.

In this study, different methods were applied in order to characterise the siliciclastic sediments and to unravel their provenance. Petrographic analyses of thin sections deliver valuable information about the mineral composition. Furthermore, the application of Quartz–Feldspar–Lithoclast (QFL) diagrams assigns the samples to a certain provenance area. X-ray fluorescence (XRF) measurements provide new geochemical data for the Triassic and Jurassic siliciclastic sediments. Major and trace element characterizations were employed to discriminate the samples from the three study areas. Heavy mineral analysis has also been applied since it is a useful technique to determine potential source lithologies (Pettijohn, 1941; Mange and Maurer, 1992; Morton and Hallsworth, 1994, 1999). However, heavy

mineral assemblages are sensitive to processes that occur during the sedimentary cycle (e.g., weathering, diagenesis, burial), and thus, they often do not reflect the original composition of the source area (e.g., Morton and Hallsworth, 1994, 1999). Therefore, different heavy mineral values using minerals with similar mechanical stability and hydraulic properties were calculated. Because zircon is present in almost all siliciclastic sedimentary rocks and it has a strong chemical and physical stability (e.g., Hubert, 1962), detrital zircon U–Pb geochronology is an important method in modern provenance analysis (e.g., Fedo et al., 2003; Meinhold et al., 2010a, 2011, 2013). The U–Pb dates of the detrital zircons yield new information on the stratigraphic ages of the Triassic and Jurassic redbeds. Furthermore, they identify potential basement complexes as sources for the detrital material, and thus, together with the other data, they contribute to the reconstruction of sediment transport paths and the palaeogeography of central Mexico during the Mesozoic.

## 2. Geological setting

### *2.1. The Mesozoic evolution of central Mexico*

Central Mexico is the interface of two different stratigraphic and tectonic regimes. The evolution of the eastern Gulf of Mexico province and the western Pacific Mexico province (Goldhammer, 1999) or the Mesozoic Atlantic Sytem and the Mesozoic Pacific System (Martini and Ortega-Gutierrez, 2016) affected its stratigraphic and tectonic evolution. The development of the Gulf of Mexico province was affected by rifting and extension of Pangaea succeeded by break-up, sea-floor spreading and subduction (Pindell and Dewey, 1982; Marton and Buffler, 1994, Dickinson and Lawton, 2001; Pindell and Kennan, 2009, Martini and Ortega-Gutierrez, 2016). The main factor controlling the tectonic evolution was the development of the passive margin related to the opening of the Gulf of Mexico in the Jurassic (Stern and Dickinson, 2010) and the Laramide orogeny in the Late Cretaceous and Cenozoic (English and Johnston, 2004; Fitz-Díaz et al., 2017). The stratigraphic phase was controlled by eustatic sea level oscillations resulting in different depositional areas. These different depositional areas are consistent with Middle-Upper lowstand deposits including redbeds, evaporites, marginal-marine siliciclastic rocks and low-relief, shallow marine high-energy carbonates (Goldhammer et al., 1991). Lower Cretaceous highstand deposits consist of high-relief, shallow-marine carbonate platforms, deep marine shales and pelagic carbonates (Goldhammer et al., 1991).

In contrast, the evolution of the western Pacific Mexico province is characterized by the development of an active continental margin and Mesozoic subduction along the pacific margin (e.g., Sedlock et al., 1993, Martini and Ortega-Gutierrez, 2016). Mesozoic subduction at the Pacific margin was the driving force that influenced the basin evolution in western Pacific Mexico (e.g., Sedlock et al. 1993). The sediment supply and the developing facies types were highly affected by the tectonics of the Jurassic to Late Cretaceous Sinaloa arc (e.g., Sedlock et al., 1993). During the Mesozoic, this arc was near the Pacific margin of Mexico. According to Johnson (1989), Pacific related subduction of the Kula plate (Barboza-Gudiño et al., 2008) caused two main phases of backarc extension and backarc closure in the western Pacific Mexico province. The first phase occurred in the Late Triassic–Middle Jurassic (west of the Coahuila block) and was accompanied by the development of the Chihuahua trough and the northern Mexican rift basin ("Mexican geosyncline"). Furthermore, the first phase also affected the Gulf of Mexico province, inasmuch as the rotation of Yucatan initiated the Gulf of Mexico province rift phase (Johnson, 1989, Pindell and Deway, 1982; Marton and Buffler, 1994, Dickinson and Lawton, 2001). In the latest Jurassic, partial closure and inversion of the backarc basin occurred (Johnson, 1989, Sedlock et al., 1993, Goldhammer et al., 1999, Martini and Ortega-Gutierrez, 2016). The Early Cretaceous was characterized by the second phase of back-arc extension in the west of the Coahuila block, resulting in the deposition of volcaniclastic material in the Chihuahua trough and the northern Mexican rift basin (Dickinson, 1981). In the east of the Coahuila block, the Gulf of Mexico province was affected by subsidence (Sedlock et al., 1993). The Late Cretaceous was characterized by the Laramide orogeny and the closure and inversion of the Chihuahua trough and the northern Mexican rift basin. During the latest Cretaceous, the Sierra Madre Oriental fold belt was formed due to regional east-directed uplift of the Alisitos arc (Sedlock et al., 1993).

*2.2. Geological formations*

Geological formations in central Mexico are often highly affected by weathering. As a result, assigning rock samples to geological formations seems to be a difficult task. Nevertheless, it is certain that overall three different geological formations including the Triassic Zacatecas Formation and the Jurassic Nazas and La Joya formations were sampled in the field. Interlayered red beds comparable to the Lower Jurassic La Boca Formation, from the Sierra Madre Oriental, are considered in the Mesa Central province as part of the Nazas Formation (Figs. 2, 3). Hence, it is arguable if La Boca Formation was sampled. Different authors

provide various classifications for the stratigraphy in the Sierra Madre Oriental and the Mesa Central region (Fig. 3). Imlay et al. (1948) suggested the name Huizachal Formation for redbed strata. Mixon et al. (1959) compiled a more detailed differentiation by the separation of two different redbed units assigning the older La Boca Formation and the younger La Joya Formation to the Huizachel Group. Barboza-Gudiño et al. (2010) suggested a new classification for the stratigraphy in both areas (Fig. 3). The Mesozoic record in the Sierra Madre Oriental and the Mesa Central region begins with Triassic successions including El Alamar Formation (continental) and Zacatecas Formation (marine) (Barboza-Gudiño et al., 2010). In La Boca Canyon, near Ciudad Victoria,Tamaulipas, the Triassic El Alamar Formation is overlain by La Boca Formation, which interfingers with volcanic deposits of the Nazas Formation (Barboza-Gudiño, 2012, 2014), contrary to a description of Eguiluz de Antuñano et al. (2014) that described La Boca Formation as Triassic in age. In Galeana, Nuevo León, where ocure the more extensive outcrops of El Alamar Formation, this unit is overlain by the Middle Jurassic La Joya Formation, because no deposit of the Lower Jurassic La Boca Formation. In the entire region, the distinct Lower Jurassic, Triassic or in some cases older units are overlain unconformably by La Joya and Zuloaga formations. In the Mesa Central region, marine Triassic strata of Zacatecas Formation underlie the volcanic Nazas Formation. Similar to La Boca Formation in the Sierra Madre Oriental, La Joya and Zuloaga formations overlie the Nazas Formation in the Mesa Central.

### *2.2.1 Zacatecas Formation*

The Zacatecas Formation in the Mesa Central, first described by Burckhardt and Scalia (1905), is the deep marine counterpart of the continental El Alamar Formation defined by Barboza-Gudiño et al. (2010) in the Sierra Madre Oriental, as remnant of fluvial deposits distinct in age and distribution to other previously defined continental units in the region. Hoppe (2000) measured a ~200 m thick succession of the Zacatecas Formation northwest of Charcas. Generally, the Zacatecas Formation is composed of siliciclastic successions that consist of interstratified sandstones, siltstones, shales and conglomeratic sandstones (Barboza-Gudiño, 2012). The Zacatecas Formation, especially in the states of Zacatecas and San Luis Potosí, represents deposits that can be assigned to the submarine Potosí fan system (Centeno-García, 2005). The Nazas Formation (Fig. 3) unconformably overlies the Zacatecas Formation.

Barboza-Gudiño et al. (2004) and Venegas-Rodríguez et al. (2009) described in Real de Catorce an informal unit named “Cerro el Mazo beds”, which is a succession of quartzite, yellow to red nodular shales and interlayered "greenstone" layers. They considered it as the base of the Nazas Formation. According to new data (this study), we know that part of this succession corresponds to the latest Triassic, including massive slump deposits and amalgamated sandstone beds at the top of the Zacatecas Formation. This Upper Triassic to Lower Jurassic marine marginal sandstone and siltstone beds, represent probably subaqueous deposits occurred close to the continental shelve and seaward deposits of a possible delta related to El Alamar fluvial system. These deposits in Real de Catorce interbedded with volcanogenic rocks of the basal part of the Lower Jurassic Nazas Formation, stratigraphic relation that can be identified in other localities of the Mesa Central as an unconformity.

*2.2.2. Nazas Formation*

The Nazas Formation (Pantoja-Alor, 1972) consists of volcanic and volcano-sedimentary successions. Blickwede (2001) described a 1000 m thick volcanic succession in the Sierra De San Julián, in northern Zacatecas. The evolution of the volcanic succession is related to a volcanic arc associated with the active continental margin of southwest North America during Early to Middle Jurassic time (Barboza-Gudiño et al., 2008). Geochronological data obtained by U–Pb geochronology of detrital zircons imply that the volcanic arc was active for a period of 40 Ma during the Jurassic (Barboza-Gudiño., 2012, Lawton and Molina-Garza, 2014).

*2.2.3. La Boca Formation*

Imlay et al. (1948) first described the redbeds exposed in the Huizachal valley as Huizachal Formation. The separation of two redbed units by Mixon et al. (1959) into the older La Boca and the younger La Joya Formation, to conform the Huizachal Group, led to a more detailed differentiation. Well-developed outcrop conditions of La Boca Formation can be found in the Huizachal Peregrina anticlinorium in Tamaulipas. In La Boca Canyon, La Boca Formation consists of a 1500 m thick succession composed of red sandstone, siltstone, mudstone and interlayered polymictic matrix-supported conglomerate and conglomeratic sandstone as well as some volcanogenic layers, equivalent to the volcanic succession exposed in the Huizachal Valley and comparable in age to the Nazas Formation. The conglomeratic sandstone is thick bedded and shows well-developed curved cross lamination. The pelitic rocks are structureless.

The sandstone and siltstone exhibit well defined stratification and a fine lamination (Barboza-Gudiño 2012).

### *2.2.4. La Joya Formation*

La Joya Formation (Mixon et al., 1959) constitutes an upward-fining sequence composed of conglomerate and red sandstone to siltstone (Barboza-Gudiño, 2012). In different localities in central and northeast Mexico, the thickness of La Joya Formation varies from zero (Miquihuana, Tamaulipas or northwest of Characs, San Luis Potosí) to over 500 m (Sierra de Catorce). The base of La Joya Formation consists of polymictic conglomerate. The components were derived from volcanic, plutonic and metamorphic rocks as well as from sedimentary rocks (Barboza-Gudiño, 2012). The middle part of La Joya Formation consists of fine-grained to medium-grained sandstone whereas the overlaying unit is composed of siltstone. Generally, La Joya Formation represents an environmental change from terrestrial to marine conditions (Michalzik, 1991). La Joya Formation is Middle to early Late Jurassic in age and is overlain by Oxfordian–Kimmeridgian shallow marine carbonates of Zuloaga Formation (Fig. 3). Detrital zircon U-Pb geochronology of the lower part of La Joya Formation northwest of Real de Catorce yielded a maximal depositional age of ca. 170 Ma and Grenvillian, Panafrican, early Paleozoic, Permo-Triassic and Early Jurassic grains (Barboza-Gudiño et al., 2012; Pérez-Casillas, 2018). In the Huizachal Valley, in the Sierra Madre Oriental, Rubio-Cisneros and Lawton (2011) reported a sigle younger grain age of 163.6 ±2.6 Ma in the upper part of La Joya Formation.

### *2.2.5. Study areas*

The location of the study areas La Ballena, Charcas and Real de Catorce is shown in Figure 2. The geographical position and the distance between the study areas are important criteria to produce reliable correlations among these areas. The three study areas are located on a NE–SW profile and have a distance of ~80 km between each other (Fig. 4). La Ballena is located ~83 km to the WNW of the city of San Luis Potosí in the states of Zacatecas and San Luis Potosí. Charcas is located in the state of San Luis Potosí, 110 km to the north of the city of San Luis Potosí. Real de Catorce represents the northernmost study area and is located in the state of San Luis Potosí with a distance of approximately 150 km from the city of San Luis

Potosí. In total, 29 rock samples were collected from surface outcrops in the three study areas (Table 1).

The study area of La Ballena represents the worst outcrop conditions among the three study areas. As a result, only three samples were taken (Fig. 4). Coarse-grained sandstone to conglomerate with volcanic fragments form the base of La Ballena section. These strata have a thickness of ~150 m. volcanic rocks unconformable overlie these strata and possess a thickness of ~200 m. The top of La Ballena profile is represented by coarse-grained sandstone without volcanic fragments (unknown thickness).

At Charcas, well-developed outcrop conditions are characteristic. Charcas was divided into two study areas (San Antonio and La Medalla) and overall 11 samples were taken (Fig. 4). In San Antonio, volcanic rocks and conglomerate as well as sandstone and siltstone were sampled. The stratigraphy begins with a volcanic breccia (thickness was not measured). Fine- to medium-grained sandstone and a conglomerate overlie these rocks. Both, the sandstone and the conglomerate include volcanic fragments. This succession is overlain by very fine- to fine-grained sandstone without volcanic fragments. The top of this ~219 m thick succession is formed by siltstone including intercalated limestone horizons. The Zuloaga Formation is also present here, but was not sampled. The transition between the siltstone and Zuloaga Formation is considered as gradational. Intercalated limestone horizons assigned to the Zuloaga Formation are present in the siltstone section and thus, evident for a continuous transition. The stratigraphic profile of La Medalla begins with a fine- to medium-grained sandstone without volcanic fragments (thickness was not measured). A ~120 m thick succession with volcanic fragments starts with a conglomerate. Due to an advanced degree of weathering, the conglomerate was not sampled. The top of this ~120 m thick succession is composed of medium- to coarse-grained sandstone with volcanic fragments.

The study area of Real de Catorce is the most diverse, complicated sampling area among the three study areas, and can be divided into a lower (~ 702 m) and an upper part (~ 512 m). In total, 15 samples were taken (Fig. 4). The lower part of the Real de Catorce profile consists of siltstone. The succession continuous with thick sandstone strata composed of very fine- to medium-grained sandstone. These sandstone strata are overlain by siltstone interlayered with thick-bedded, commonly cross-laminated quartzite. The described succession does not include volcanic fragments. However, a succession of fine-grained sandstone with volcanic fragments and a highly weathered volcanic rock are also assigned to the lower part of the profile. The upper part of the profile consists of a fine sandstone with ripple marks without volcanic fragments, overlain by conglomerate and sandstone with

volcanic fragments. The top of the upper part consists of a siltstone with intercalated limestone horizons of the Zuloaga Formation. Similar to the realm of Charcas the transition between the redbeds and the overlying Zuloaga Formation is considered as transitional.

## 3. Sample description

### *3.1. Volcanic rocks*

Volcanic rocks occur in each of the three study areas. The sample LaB A2 taken in La Ballena was identified as a conglomeratic rock during the fieldwork. However, the thin section analysis indicated that this sample is a volcanic rather than a sedimentary rock. The volcanic rock sample Cha B1 taken in Charcas is a massive volcanic breccia of grey color, which is highly affected by weathering. In Real de Catorce, a red to purple massive volcanic rock (sample RdC C9) also highly affected by weathering was sampled.

### *3.2. Conglomerate*

The conglomerate often occur in reddish to light reddish or grey colors and can be described as polymictic conglomerate with sedimentary, volcanic and metamorphic clasts. The clast sizes range from 1–15 cm, whereas the shape of the clasts varies from rounded to poorly rounded to angular. The predominant fabric of the conglomeratic rocks is clast-dominated but in some cases, they also occur with a matrix-dominated fabric. The detected sedimentary structures are horizontal bedding and in some cases tabular cross bedding. The conglomeratic rock sample from La Ballena (sample LaB A1) is mostly light reddish and clast dominated. The clasts are rounded and angular. In comparison, the conglomeratic rock from Charcas (sample Cha B7) is purple to reddish and matrix dominated. Towards the base of the conglomerates an increase in clast size was detected in the field. Moreover, the clasts near the base of the conglomerate horizons are more rounded than the other clasts. The conglomeratic rock collected in Real de Catorce (sample RdC C11) is grey and clast dominated and provides the smallest clasts among the analyzed conglomeratic rocks.

### *3.3. Sandstone*

The grain size varies from fine-grained to coarse-grained, and the grains are subrounded to subangular. The grain assemblages are poorly to well sorted. The majority of the sandstones is affected by weathering and provide colors from pale grey to intense red. Characteristic sedimentary structures encompassing ripple marks and cross bedding are scarce and restricted to a few samples. Most of the analyzed sandstones do not show sedimentary structures. The cross bedding structures only occur in small scales and the stratification ranges from thin to thick beds.

### *3.4. Siltstone*

The siltstones are fine-grained and mostly red or pale grey, comoonly structureless but sometimes thin-bedded, showing graded bedding and curved cross-lamination, compossed of subangular to angular quarz and minor feldspar and lithic fragments. In some cases, fine-grained sandstone strata are interbedded with the siltstone. Intercalated limestone horizons assigned to the Zuloaga Formation are interbedded in the upper part of the siltstone section and thus, evident for a continuos transition between the siltstone and the overlying limestone of the Zuloaga Formation, which is considered as gradational.

## 4. Sample preparation and analytical methods

For simplification, the term LaB is used for the samples collected in La Ballena, Cha for the samples collected in Charcas and RdC for the samples colected in Real de Catorce. The samples were prepared for different analytical purposes including petrographic analysis, geochemical and heavy mineral analysis as well as for detrital zircon U–Pb geochronology. Details about sample preparation and analytical methods are found in Appendix 1. Petrographic data are given in Table 2. The full set of analytical data is given as supplementary data.

## 5. Results

### *5.1. Petrographic analysis*

Petrographic analysis is an extremely valuable technique to determine the mineral composition of different lithologies. The volcanic rock samples were also described in thin

sections but only sandstone and coarse-grained siltstone samples were counted and used for the Quartz–Feldspar–Lithoclast (QFL after Dott, 1964, Weltje, 2006) analysis (Figure 5 and Table 2).

### *5.1.1. Volcanic rocks*

The thin section analysis revealed that LaB A2 is a weakly deformed volcanic rock that contains numerous plagioclase crystals. The plagioclase occurs as well developed, long and thin laths. The fabric of the plagioclase laths shows a preferred orientation with a distinctive shear motion.

Sample Cha B1 is a volcanic breccia with subrounded to subangular grains. This sample consists of feldspar, volcanic and metamorphic fragments. The most abundant feldspar grains are plagioclases. The plagioclase laths within the volcanic fragments are mostly small. Furthermore, K-feldspar grains are mostly broken. This might be indicative of mechanical stress.

Sample RdC C9 is a volcanic rock and mostly consists of opaque minerals as well as plagioclase between the opaque minerals. Notably, the plagioclase provides a fabric that might be the result of weak deformation. Furthermore, the opaque minerals offer a preferred orientation accorded to the deformation structures.

### *5.1.2. Sedimentary rocks - QFL analysis*

Samples from the Zacatecas Formation are quartz arenites and sublitharenites (Fig. 6). A sandstone sample from the Nazas Formation is classified as lithic arenite, and samples from La Joya Formation are more diverse, being classified as quartz arenites, subarkoses, arkosic arenites, sublitharenites, and lithic arenites. The majority of all samples plot in the field of recycled orogen provenance. With a few exceptions, samples from Nazas and La Joya formations are characterized by feldspar and volcanic lithoclasts whereas samples from Zacatecas Formation only contain minor amouts of feldspar and lack volcanic lithoclasts (Table 2).

## *5.2. Geochemistry*

Whole-rock geochemical analysis of major and trace elements was carried out to determine element concentrations in order to characterise the different lithologies. From the three volcanic rock samples, only two samples were analyzed by XRF. Note that for the sedimentary rock samples the data are not used for an in-depth geochemical interpretation since the samples show signs of alteration (likely due to weathering). The mobility of major elements during weathering and diagenetic processes can be seen as a disadvantage (Rollinson, 1993; Armstrong-Altrin and Verma, 2005). Hence, discrimination diagrams for lithology, provenance and tectonic setting utilising major elements have to be used with great care to avoid misleading interpretations. Trace elements mostly react immobile under surface conditions and hence trace element data can be considered to be more reliable (e.g., Zimmermann and Bahlburg, 2003).

### *5.2.1. Volcanic rocks*

The samples (Cha B1, RdC C9) can be distinguished on the basis of major element concentrations. However, due to the advanced degree of weathering of the volcanic rocks analyzed in this work, it is questionable if the major element data are reliable. Generally, the high mobility of alkaline elements during secondary processes limits the application of the TAS diagram [($Na_2O + K_2O$) vs. $SiO_2$] to fresh and mostly unweathered volcanic rocks (e.g., Barboza-Gudiño et al., 2008). The mobility of an element depends on the charge/radius values (ionic potential). Elements with a low ionic potential are more easily removed than elements with a high ionic potential. An intermediate ionic value enables elements to remain in the solid phase (Pearce, 1996). Therefore, the volcanic rocks were classified using trace element values ($Zr/TiO_2$ and Nb/Y) including immobile elements (Winchester and Floyd, 1977). Sample Cha B1 can be classified as rhyolite and sample RdC C9 as rhyodacite/dacite. Regardless of the diagrams used, the samples are subalkaline intermediate and acidic volcanic rocks.

### *5.2.2. Sedimentary rocks*

Due to possible mobility of major elements, we will only focus on selected trace elements. The Th/Sc vs. Zr/Sc diagram after McLennan et al. (1993) is shown in Figures 7a and can be used to evaluate igneous chemical differentiation processes and the degree of sediment recycling consistent with zircon enrichment (McLennan et al., 1993; Meinhold et al., 2007).

The Th/Sc value is a useful indicator of magmatic differentiation processes because Th is an incompatible element and thus, enriched in felsic rocks, whereas Sc is compatible in igneous systems. The Zr/Sc value reflects the degree of sediment recycling, inasmuch as a high Zr/Sc value is indicative of high sediment recycling and weathering rates (McLennan et al., 1993). The majority of the analyzed samples illustrate intermediate Th/Sc and Zr/Sc values, with Th/Sc of 0.14−1.28 and Zr/Sc of 4.6−62 respectively, suggesting no significant reworking and zircon enrichment.

The discrimination diagram by Floyd and Leveridge (1987) uses La/Th vs. Hf to classify different arc compositions and sources. Referring to Figure 7b, the analyzed samples are primarily located in the acidic arc source field or at least very close to this field. A single sample from the La Joya Formation tends towards an andesitic arc source.

In Figure 7c, Cr and Ni values are used to identify a possible ultramafic (ophiolitic) input derived from the source area (Garver et al., 1996; Meinhold et al., 2009). The majority of the samples contain low Cr and Ni values (<150 ppm Cr and <100 ppm Ni). Interestingly, the two sandstone samples from the Zacatecas Formation and the single sandstone sample from the Nazas Formation show high Cr and Ni values similar to the volcanic rock sample RdC C9 from the Nazas arc.

*5.3. Heavy mineral analysis*

In total, the heavy mineral content of 2 volcanic rock samples and 15 sedimentary samples was analyzed. Generally, 250 heavy mineral grains were counted in heavy mineral slides using a polarising microscope (Zeiss Axioplan2). The heavy mineral abbreviations used in this study are according to Whitney and Evans (2010). The main translucent heavy minerals detected in the studied samples are pyroxene (Px), amphibole (Amp), epidote (Ep), sphene (Spn), garnet (Grt), chlorite (Chl), tourmaline (Tur), apatite (Ap), anatase (Ant), rutile (Rt) and zircon (Zrn) (Fig. 8). Both, clino- and orthopyroxene occur in the samples but they have not been separately counted. Chlorite, epidote and mica are often attached to opaque minerals. Garnet occurs only in a few samples; the grains are colorless and are mostly angular and irregular fragments. Apatite grains occur in angular and subrounded forms. They are colorless or reddish-brown. Anatase grains are yellow to pale brown with an angular shape. Rutile grains are red-brown. They mostly occur as prismatic grains or as fragments of prismatic grains. Zircon grains are rounded or show well developed prismatic shapes. They are colorless or pale pink.

Heavy mineral analysis is one of the most sensitive and widely used method to determine possible provenance areas of sandstones (e.g., Mange and Maurer, 1992; Morton and Hallsworth, 1994, 1999). However, heavy minerals are sensitive to processes that occur during weathering. Hence, they often do not reflect the original composition of the source area (Morton and Hallsworth, 1994). The most abundant translucent heavy minerals, zircon and apatite, appear in nearly all samples in different abundances. Samples from the Zacatecas Formation and from the lower part of the La Joya Formation have a high abundance of zircon. The volcanic rock sample Cha B1 contains more zircon (6 %) and apatite (18 %) compared to sample LaB A2 (zircon: 1.6 %, apatite: 1.2 %). Remarkably, a decrease of apatite referring to the geographical position of the study areas can be recognised. Apatite decreases from SW (La Ballena) to NE (Real de Catorce) (Fig. 8). Further differentiations can be made on the basis of pyroxene. Generally, the pyroxene abundance is low in all samples. Nevertheless, with the exception of sample RdC C2, samples from the Zacatecas Formation show greater abundances of pyroxene than those of the other formations.

Heavy mineral assemblages are highly affected by processes occurring during weathering, transport, deposition and diagenesis. These processes have the capability to alter the heavy mineral composition before their incorporation into the sediment. Hence, analysis only based on the variety of heavy mineral compositions may not reflect the original heavy mineral composition of the source area (Morton and Hallsworth, 1994, 1999). The application of heavy mineral values including minerals with similar mechanical stability and hydraulic behaviour is a useful tool to characterise the source area (Morton and Hallsworth, 1994, 1999). The mechanical stability and hydraulic behaviour depends especially on grain size, grain density and grain shape (Morton and Hallsworth, 1994, 1999).

Provenance-sensitive heavy mineral index values were calculated as suggested by Morton et al. (2005): ATi (apatite: tourmaline index), RuZi (rutile:zircon index), and GZi (garnet:zircon index). In addition, the ZTR index (zircon, tourmaline, rutile) was calculated as defined by Hubert (1962) (Fig. 9). The ATi index ranges from 0 to 100 and exceeds 70 in the most cases. Sample Cha B9 provides values below 50 resulting from the highest tourmaline abundances among all samples. The samples LaB A2, Cha B1, Cha B5, Cha B7, Cha B8, Cha B10 as well as RdC C2 have no tourmaline and hence, yielded ATi values of 100. Sample RdC C8 has neither tourmaline nor apatite. The calculated RuZi index shows variations among the volcanic rock samples. The sample LaB A2 contains no rutile and thus, the RuZi cannot be calculated. However, sample Cha B1 reveals a RuZi of 6.3 (Fig. 9). RuZi values range from 0–8.5 (Fig. 9). Due to a lack of rutile grains, it was impossible to calculate the

RuZi values for samples Cha B6, Cha B7 and Cha B11. RuZi is not appropriate to distinguish the sediments with regard to the three formations since values are roughly similar. These values result from approximately similar rutile abundances. In contrast, GZi seems to be a useful parameter to distinguish the sediments. The volcanic rock samples (LaB A2, Cha B1) do not contain garnet; hence, GZi values could not be calculated. Sandstones from the Zacatecas and Nazas formations reveal very low GZi (0–3.2) resulting from low abundances of garnet, accompanied by high zircon contents. However, a lack of garnet grains made it impossible to calculate the GZi for the samples Cha B9, RdC C2 and RdC C6a. On the contrary, sandstones from La Joya Formation show greater GZi values (0–36.4) resulting from higher garnet contents and lower zircon abundances. The samples Cha B6 and Cha B7 show GZi values >30 resulting from high garnet contents and the lowest zircon abundances among the samples from La Joya Formation. The samples Cha B11 and RdC C8 do not contain garnet grains; hence, their GZi is zero. The ZTR index is high in samples from the Zacatecas Formation, low in samples from the Nazas Formation, and variable for samples from the La Joya Formation (Fig. 9). There is no correlation between ZTR and whole-rock $SiO_2$ content.

*5.4. Detrital zircon U–Pb ages*

The method of U–Pb geochronology was applied to determine provenance areas and the maximum depositional age of the samples. Zircon cores and rims were analyzed (Fig. 10). Dickinson and Gehrels (2009) suggested that the maximum depositional age can be inferred from the youngest age population including the youngest zircon age cluster. The geologic time scale of Gradstein et al. (2012) was used as stratigraphic reference for data interpretation. Length-to-width values (L/W) were calculated to identify possible correlations between grain shape (aspect ratio) and U–Pb age. However, no correlation between L/W values and U–Pb ages have been recognised.

A total number of 323 U–Pb zircon ages have been obtained from 319 zircon grains, of which 252 zircon ages are 95–105 % concordant. Table 3 reveals a summary of weighted average ages of the youngest zircon age populations as well as the youngest grain ages. Figure 11 illustrates histograms and kernel density estimation curves for all samples. Sedimentary rocks of the Zacatecas Formation are characterized by Late Triassic ages (weighted average ages: 215. ± 6 Ma to 205 ± 10 Ma) in the youngest age group. Taking the weighted average ages and the youngest grain ages into account, the samples Cha B9 and RdC C4 reveal Norian

ages, which are also consistent with the youngest grain ages provided by these samples (Table 3). Sample RdC C6a shows an earliest Jurassic age (around the Sinemurian–Hettangian boundary). Sample RdC C8 from the Nazas Formation illustrates an Early Jurassic age (Pliensbachian-Toarcian boundary, accord to Walker et al. (2018). Samples from the La Joya Formation reveal Early to Middle Jurassic ages (weighted average age: 165.2 ± 3.6 Ma to 187.7 ± 3.1 Ma). The weighted average ages of samples Cha B8 and Cha B6 reveal Middle Jurassic ages including the stages Callovian (Cha B6) and Aalenian (Cha B8). These observations are consistent with the youngest grain ages provided by these samples. Overall, the zircon data contain seven age populations that occur at ~1780–1300 Ma, 1290–900 Ma, ~720–450 Ma, ~445–310 Ma, ~300–240 Ma, ~240–200 Ma, ~200–150 Ma (Fig. 11). The results for the U–Pb geochronology for the analyzed samples are summarised in Tables S7–S13 (see Supplementary data).

Zacatecas Formation, sample RdC C4: In total, 83 zircons were analyzed, with 66 zircons providing concordant ages. The results reveal three major age populations at ~330–210 Ma, ~1275–900 Ma and ~1350–1225 Ma. Significant peaks within the youngest age population occur at ~225–200 Ma, ~300–240 Ma, whereas two minor peaks appear at ~350–300 Ma. The very youngest zircons reveal a cluster at ~250–210 Ma including a major peak at ~220– 215 Ma. The second oldest population provides Neoproterozoic to Mesoproterozoic ages with several peaks. However, the most prominent peaks occur at ~965–940 Ma and ~1100–1075 Ma. The most conspicuous peak of the oldest age population (Mesoproterozoic) appears at ~1285–1260 Ma. Furthermore, eight minor age populations occur at 392 ± 13 Ma, ~450±25 Ma, 585 ± 19 Ma, 719 ± 17 Ma, 1399 ± 26 Ma, 1448.5 ± 9.9 Ma, 1525 ± 22 Ma, 1782.1 ± 9.7 Ma. The majority of the analyzed zircons illustrate concentric zoning. Cores can be recognised only in a few zircon grains. With the exception of zircon C4_2, the Th/U values are higher than 0.1 ppm. The calculated length-to-width values (L/W) range from 0.88–4.31.

Zacatecas Formation, sample RdC C6a: In total, 94 zircons were analyzed, with 78 zircons providing concordant ages. The results reveal four major age populations at ~220–199 Ma, ~328–220, ~725–400 Ma, and ~1275–950 Ma. A Significant peak within the youngest age population occurs at ~265–240 Ma. The very youngest zircons reveal a cluster at ~250–190 Ma including a major peak at ~250–245 Ma. The youngest grain in this sample provides an age of 199.1 ± 8.5 Ma (Table 3). Thus, this grain illustrates an age around the Hettangian–Sinemurian boundary. However, referring to Tables S10 (see Supplementary data); only two zircon grains illustrate Early Jurassic ages. The remaining zircon clusters offer Triassic and older ages. The second oldest population provides a wide range of ages, from Early Devonian

to Neoproterozoic ages including conspicuous peaks at ~475–425 Ma. The oldest age population offers Neoproterozoic to Mesoproterozoic ages and the most conspicuous peaks yield ages at ~1025–1000 Ma and ~1065–1040 Ma. Furthermore, three minor age populations occur at 1518 ± 14 Ma, 1576 ± 14 Ma and 1665 ± 11 Ma. Most of the measured zircons show concentric zoning, whereas the occurrence of cores is lacking in most cases. The Th/U values are higher than 0.1 ppm. The calculated length-to-width values (L/W) range from 0.83–4.09.

Zacatecas Formation, sample Cha B9: In total, 59 zircons were analyzed, with 52 zircons providing concordant ages. The results reveal four age populations at ~325–210 Ma, 600–420 Ma, ~1300–920 Ma and ~1520–1320 Ma. However, one zircon grain yields an age of 1668 ± 13 Ma. The youngest age population includes several significant peaks between ~300 and ~225 Ma, with the most prominent peak at ~250–245 Ma. The oldest age population has a wide range and represents Neoproterozoic to Paleoproterozoic ages including several peaks. The most conspicuous peaks occur at ~985–960 Ma, ~1050–1052 Ma, and ~1250–1225 Ma. One zircon grain was used to determine the age of the core (spot B9_43: 1076 ± 20 Ma) and the rim (spot B9_42: 968 ± 20 Ma). Most of the analyzed zircons reveal concentric zoning. Furthermore, cores can be recognised in a few zircon grains. The Th/U values are mostly higher than 0.1 ppm. The calculated length-to-width values (L/W) range from 0.57–3.47.

Nazas Formation, sample RdC C8: A total number of 45 zircons were analyzed, with 33 zircons providing concordant ages. The results reveal five age populations at ~195–180 Ma, ~280–200 Ma, ~565–440 Ma, ~1255–960 Ma and ~1400–1260. Significant peaks within the youngest age population occur at ~200–175 Ma and ~270–145 Ma. The very youngest zircons reveal a cluster at ~210–180 Ma including a major peak at ~185–190 Ma. The youngest grain in this sample provides an age of 182.8 ± 8.7 Ma (Table 3). Thus, the youngest grain illustrates an Early Jurassic (Pliensbachian) age. The oldest age population offers Neoproterozoic to Mesoproterozoic ages, and the most conspicuous peaks occur at ~975–950 Ma, ~1180–1155 Ma, ~1260 –1235 Ma and ~1325–1300 Ma. Three zircon grains were used to determine the age of the core and the rim (spot C8_1 c: 188 ± 5.6 Ma, spot C8_2 r: 187.3 ± 5.4 Ma; spot C8_17 c: 1535 ± 19 Ma, spot C8_18 r: 443 ± 14 Ma; spot C8_20 c: 992 ± 21 Ma, spot C8_21 r: 561 ± 15 Ma). The majority of the analyzed zircons provide concentric zoning as well as cores. The Th/U values are mostly higher than 0.1 ppm. The calculated length-to-width values (L/W) range from 1.13–4.02.

La Joya Formation, sample Cha B8: Unfortunately, zircons were very scarce in this sample. Hence, a total number of only 7 zircons were analyzed, with 4 zircons providing

concordant ages. The results reveal only two age populations at ~180–155 Ma and 1042 ± 45 Ma. The youngest age population illustrates a distinct peak at ~175–170 Ma, which is consistent with the youngest grain (171 ± 6.2 Ma) within this sample (Table 3). Concentric zoning and cores appear in a very few cases. The Th/U values are mostly higher than 0.1 ppm. The calculated length-to-width values (L/W) range from 0.75–2.6.

La Joya Formation, sample Cha B6: Unfortunately, zircons were very scarce in this sample. Hence, a total number of only 7 zircons were analyzed, with 5 zircons providing concordant ages. The results reveal 4 age populations at ~175–150 Ma, 435.7 ± 8.8 Ma, 579 ± 17 Ma and 1188 ± 22 Ma. The youngest age population illustrates a distinct peak at ~170–165 Ma, which is consistent with the youngest grain (165.2 ± 4.9 Ma) within this sample (Table 3). The majority of the zircons illustrate concentric zoning, whereas cores are scarce. The Th/U values are higher than 0.1 ppm. The calculated length-to-width values (L/W) range from 1.2–3.62.

La Joya Formation, sample LaB A3: In total, 24 zircons were analyzed, with 17 zircons providing concordant ages. The results reveal only one significant age population at ~240–145 Ma. This population includes an accumulation of ages at ~175–145 Ma and three minor age populations at 183.4 ± 4.4 Ma, 205.2 ± 6.8 Ma and 240 ± 8 Ma. In addition, 3 minor age populations at 902 ± 24 Ma, 1000.7 ± 9.2 Ma and 1322 ± 39 Ma represent Neoproterozoic to Mesoproterozoic zircon ages. Figure 12 reveals a Concordia diagram including the samples taken for the mean age calculation. Taking the histograms, the concordia diagram as well as the calculated mean age of the youngest zircon age population into account, sample LaB A3 provides a Late Jurassic (Oxfordian to Kimmeridgian) age. The majority of the analyzed zircons show concentric zoning. The Th/U values are higher than 0.1 ppm. The calculated length-to-width values (L/W) range from 0.82–3.27.

Figure 11 shows the occurrence of a wide range of zircon populations in samples from the Zacatecas Formation, compared to those belonging to the Nazas Formation and mainly to La Joya Formation, which has only a few minor peaks with a main population, coincident or very close to the maximum age of the deposit. The above, supports the criteria for tectonic discrimination proposed by Cawood et al. (2012), who point out a direct relation of the detrital zircons population and the proportion of detrital zircons aged close to the age of deposition, where a greater proportion of ages close to the maximum age of the deposit are indicative of convergent plate margins (La Joya and Nazas formations, as deposits in a possible arc and back-arc), and sediments in collisional, extensional and intra-cratonic settings, characterized by a greater proportion of different and older ages that reflect the

history of the basement (Zacatacas Formation as deposits in an ancient extensional or passive margin).

## 6. Discussion

### *6.1. Petrographic analysis*

In total, 27 thin sections including 3 volcanic rocks and 24 sediments were analyzed (Table 1). The volcanic rocks contain large amounts of plagioclase laths indicating derivation from a felsic to intermediate source. The rocks are identified as rhyolite (Cha B1) and dacite (RdC C9). These observations are consistent with results obtained from volcanic rock samples assigned to the Nazas arc (Barboza-Gudiño et al., 2008). The sample Cha B1 can be described as volcanic breccia possibly derived from a pyroclastic flow. The occurrence of a volcanic breccia in the realm of Charcas might be indicative of volcanic activity and sedimentation processes at the same time. A volcanic breccia from Aramberri (Nuevo Leon) described by Barboza-Gudiño et al. (2008) can be compared with the volcanic breccia analyzed in this study (Cha B1). Both samples are composed of subangular (Cha B1) to angular grains (sample analyzed by Barboza-Gudiño et al., 2008) and provide a rhyolitic composition. Comparing the thin sections of samples LaB A2 and RdC C9 (identified as dacite), especially under crossed polars, similarities are recognisable. Both samples contain large amounts of plagioclase leading and texturally and mineralogically LaBA2 and RdCC9 look similar so the former might also be a dacite. However, sample LaB A2 was not analyzed by XRF. Hence, this assumption needs to be confirmed by geochemical analysis. Furthermore, samples RdC C9 and LaB A2 reveal structures of weak deformation, which are possibly caused by the Late Cretaceous to the Paleocene (80–55 Ma) Laramide Orogeny (English and Johnston, 2004). All studied sediments samples are quartz rich with variable amounts of feldspar and volcanic fragments (Fig. 6). With a few exceptions, samples from the Nazas and La Joya formations are characterized by feldspar (plagioclase dominates over K-feldspar) and volcanic fragments whereas samples from the Zacatecas Formation only show minor amouts of feldspar and lack very scarce volcanic fragments (Table 2). This observation may be useful in future studies since assigning of rock samples based on field observations to Triassic or Jurassic geological formations is anything but straightforward and needs to be confirmed by further investigations. The volcanic fragments contain large amounts of plagioclase laths. Probably, these plagioclase laths are comparable to those within the volcanic rocks indicating derivation

from the Nazas arc. The lack of volcanic fragments in some of the La Joya Formation sediments accompanied by low feldspar contents (Cha B4, Cha B5, RdC C10) suggest sediment supply from the Zacatecas Formation.

With a few exceptions, sediments from the La Joya Formation illustrate significantly higher feldspar abundances than those from the Zacatecas Formation (plagioclase dominates over K-feldspar). This might either be indicative for higher weathering rates in the source area of the Zacatecas Formation or for stronger weathering conditions after the depositional processes. The sediments without volcanic fragments plot on the transition between the quartzarenite, subarkose and sublitharenite fields.

*6.2. Geochemistry*

Whole-rock geochemical data were obtained by XRF analysis. The volcanic rocks are intermediate to acidic in composition and are classified, employing trace elements data according to Winchester and Floyd (1977), as rhyolite (sample Cha B1) and dacite (sample RdC C9).

The studied sediments were most likely derived from a felsic to intermediate source. Depletions in Cr and Ni preclude input from mafic/ultramafic rocks (ophiolitic source). Th/Sc vs. Zr/Sc reveals low sediment recycling. However, zircon grains are significantly enriched in samples from the Zacatecas Formation (according to heavy mineral analysis) indicating stronger sediment recycling rates.

*6.3. Heavy mineral analysis*

In the analized samples, generally, translucent heavy minerals are more abundant in sediments without volcanic fragments and scarce in the volcanic or volcaniclastic rocks. Although abundances of translucent minerals, including the majority of the heavy minerals (Pxn Amp, Ep, Spn, Grt, Chl, Tur, Rt, Ant) are scarce in all samples (Fig. 8). The most abundant heavy minerals occurring in the samples are zircon and apatite. The sediments without volcanic fragments illustrate higher zircon abundances compared to the sediments with volcanic fragments; whereas apatite is more abundant in sediments with volcanic fragments, with the exception of intermediary to mafic volcanic rocks, which show uncommon chlorite and in some cases epidote.

Hence, provenance discrimination based on these heavy minerals is impossible. The most important parameters influencing heavy mineral assemblages are hydraulic sorting and diagenesis (Morton and Hallsworth 1994). The hydraulic behaviour of a single grain depends on grain density, grain shape and grain size (Morton and Hallsworth, 1994, 1999). Morton and Hallsworth (1994) documented that heavy minerals with different habits have different hydraulic properties. Therefore, for provenance analysis, the best results are obtained from minerals with similar habits. Processes occurring during diagenesis and burial (e.g., dissolution) are often accompanied by losing unstable heavy minerals (Morton and Hallsworth, 2007). The main factor causing dissolution of heavy minerals during diagenesis and burial is the pore fluid temperature (Morton and Hallsworth, 2007). Referring to Morton and Hallsworth (1994, 1999, 2007), an increase in burial depths is accompanied by an increase in pore fluid temperature. The combination of increasing temperatures and the change of the pore fluid composition is responsible for dissolution processes of unstable heavy minerals. According to Morton and Hallsworth (2007), the relatively low abundances of the unstable heavy minerals might be caused by burial and dissolution. On the basis of several case studies, Morton and Hallsworth (2007) compiled the relative stability of detrital heavy minerals in deep burial conditions. Pyroxene (CPx, OPx) and amphibole grains are highly unstable in the subsurface. Epidote grains are more stable than amphibole grains but are also unstable in the subsurface. Sphene is more stable than amphibole and epidote grains, but is also unstable in the subsurface (Morton and Hallsworth, 2007). Garnet is a common mineral in metamorphic rocks and considered to be more stable under deep burial conditions than the previously discussed heavy minerals. However, dissolution processes of garnet under deep burial conditions were recognised by Morton (1984). Furthermore, the occurrence of acidic groundwater during weathering can lead to dissolution of garnet (Morton and Hallsworth, 2007) and apatite (Morton, 2012). Hence, the low abundances of garnet in the studied samples can likely be attributed to a lack of garnet-bearing rocks in the source area(s) but not to weathering caused by acidic groundwater since apatite is still present. La Joya Formation sediments illustrate greater GZi values than Zacatecas Formation sediments caused by higher zircon abundances in the latter (Fig. 9). However, the GZi value may not reflect the original composition of the source area because garnet grains possibly disappeared during burial and weathering. Tourmaline is a common mineral in magmatic rocks, hydrothermal mineral deposits as well as in metamorphic rocks and is very stable during weathering and transport. Morton and Hallsworth (2007) documented that dissolution of tourmaline appears at depths exceeding 4 km and is most likely caused by a combination of depth and unusual

fluid composition. Tourmaline is very rare in all samples. Rutile grains often occur in metamorphic rocks (Meinhold, 2010) and according to Turner and Morton (2007), there is no evidence for dissolution processes during diagenesis. Generally, the scarcity of metamorphic minerals in the heavy mineral spectrum might either be indicative for a lack of metamorphic source rocks or for dissolution processes after deposition of the sediment. The lack of metamorphic input can also be inferred from the calculated Th/U values of the detrital zircon grains. Including all analyzed detrital zircon samples, the calculated Th/U values are predominantly higher than 0.1 indicating magmatic rather than metamorphic input (Rubatto, 2002; Meinhold et al., 2008). The most abundant heavy minerals occurring in the samples are zircon and apatite. Zircon is a common mineral in felsic and intermediate igneous rocks and is considered to be stable in sandstones and in general during burial (Hubert 1962, Morton and Hallsworth 2007). Remarkably, Zacatecas Formation sediments illustrate higher zircon abundances compared to La Joya Formation sediments (Fig. 8). Taking the stability during burial and weathering into account, higher zircon abundances might be indicative for higher sediment recycling rates in the source area(s). Hubert (1962) argued that the ZTR (zircon, tourmaline, rutile) index reflects the mineralogical maturity of sandstones. With regard to the Zacatecas Formation sediments, high zircon abundances, low tourmaline and low rutile abundances result in high ZTR indices (Fig. 9). In contrast, lower zircon abundances, low tourmaline and rutile contents lead to low ZTR values including the sediments with volcanic fragments (La Joya Formation). According to Hubert (1962), zircon, tourmaline and rutile are concentrated with quartz and chert. High ZTR indices in the Zacetacas Formation sediments are consistent with high total quartz abundances. This observation probably marks a change in provenance, inasmuch as the source area(s) for the Zacatecas Formation sediments can be characterized by a greater maturity. Apatite grains are considered very stable during transport and burial. However, apatite is highly sensitive to surficial weathering (Morton, 1986, 2012). The decrease of apatite from the southeast (La Ballena) towards the northeast (Real de Catorce) might be indicative of stronger weathering conditions in the vicinity of Real de Catorce. Another likely approach to explain the scarcity of apatite in Real de Catorce is a different source area compared to La Ballena and Charcas.

### *6.4. Detrital zircon U–Pb ages*

The results obtained from the U–Pb geochronology provide a wide range of ages. Age populations occur at ~1780–1300 Ma, ~1290–900 Ma, ~720–450 Ma, ~445–310 Ma, ~300–

240 Ma, ~240–200 Ma, ~200–150 Ma (Fig. 11). The oldest age population within the samples (~1780–1300 Ma) illustrates Palaeoproterozoic–Middle Mesoproterozoic ages. This age population makes up 10 % of 252 concordant zircon ages. With the exception of sample RdC C8 (Nazas Formation), the occurrence of this age population is restricted to the Zacatecas Formation. Based on zircon cores providing Palaeoproterozoic–Mesoproterozoic ages, Ortega-Flores et al. (2014) suggested that zircons of these ages were possibly derived from the Huiznopala gneiss. The Huiznopala, Novillo and Guichicovi gneisses together with the Oaxacan complex make up the Oaxaquia microcontinent of Mexico (Keppie et al., 2003), which is a vestige of the Grenvillian belt (~1250–900 Ma) (e.g., Weber et al., 2012). Weber et al. (2012) assume that the Palaoeproterozoic–Mesoproterozoic provinces of Amazonia were likely attached to the Oaxaquia microcontinent during its development. A further probable approach to explain the oldest zircon population proposes that sedimentary detritus directly derived from the Rio Negro-Juruena (~1800–1550 Ma) province of western Amazonia (Ortega-Flores et al., 2014).

The second oldest age population illustrates ages ranging from ~1290–900 Ma (Middle Mesoproterozoic–Early Neoproterozoic) and represents the most abundant age population (39 % of 252 concordant zircon ages). This population is present in all samples but shows greater abundances in the Zacatecas Formation. The detrital input responsible for these ages probably originated from basement rocks with Grenvillian affinity present in the Oaxaquia microcontinent.

Late Neoproterozoic–Ordovician ages are represented by the ~720–450 Ma age population and occur in all analyzed samples. This age population makes up 9 % of 252 concordant zircon ages and is indicative for the Pan-African orogeny (Rino et al., 2008) and Early Palaeozoic tectono-magmatic events. The Maya (Yucatan–Chiapas), Chortis, Oaxaquia, Coahulia and Florida blocks were accreted to Gondwana during its final assembly and are considered as possible source areas (Dickinson and Lawton, 2001, Murphy et al., 2004).

A further age population provides ages ranging from ~445–310 Ma (Late Ordovician–Pennsylvanian) and makes up 6 % of 252 concordant zircon ages. The nearest possible source areas are the Acatlán Complex and the Maya (Yucatan–Chiapas) block where Early Palaeozoic igneous rocks are present (Steiner and Walker, 1996; Nance et al., 2009; Martens et al., 2010). Recycling from pre-Permian low-grade metasedimentary rocks containing early Palaeozoic zircon grains is also possible. Low-grade metasedimentary rocks with Early Palaeozoic detrital zircons are known, for example, from the Acatlán Complex (Nance et al., 2009). It is noteworthy that the occurrence of the ~445–310 Ma age population is restricted to

the Zacatecas Formation. Despite low abundances of this population within the sediments without volcanic fragments, it suggests the existence of a source area that delivered detritus exclusively for the Zacatecas Formation.

Permian–Triassic ages are presented by an age population ranging from ~300–240 Ma and make up 18 % of 252 concordant zircon ages. Referring to Ortega-Flores et al. (2014), the detrital zircons yielding these ages derived from a continental magmatic arc located on the western margin of Pangaea. The magmatic activity of this arc occurred from 300–235 Ma (Torres et al., 1999, Dickinson and Lawton, 2001Stern and Dickinson, 2010, Barboza-Gudiño et al., 2010). With the exception of sample RdC C8 (Nazas Formation), this age population is only present in the Zacatecas Formation. Ortega-Flores et al. (2014) described Triassic sandstones of the El Chilar Complex of the Tolimán area (west of the Sierra Madre terrene) without volcanic fragments and great abundances of Permian–Triassic zircons. This observation is consistent with the samples from the Zacatecas Formation analyzed in this study because they contain high abundances of Permian–Triassic zircons and have no volcanic fragments.

The second youngest population within the samples is represented by ~240–200 Ma-old zircon grains, which make up 7 % of 252 concordant zircon ages. This age population may represent an event related to the breakup of Pangaea and initial rifting that formed the Gulf of Mexico (Steiner and Walker, 1996). The ages might be related to the initial stage of the Nazas magmatic arc (~232–150 Ma: Stern and Dickinson, 2010). The nearest Late Triassic igneous rocks are exposed to the east of the study area, in the Sierra Madre Oriental fold and thrust belt, e.g., ~220 Ma-old Acatita intrusives (Molina-Garza, 2005). However, it is uncertain if these rocks were already exposed on the surface in latest Triassic and Jurassic times to supply detrital material for the studied sediments. Notably, the occurrence of this population is mainly restricted to the Zacatecas Formation. However, sample RdC C8 from the Nazas Formation also contains this population. In total, zircon grains providing these ages are scarce but suggest a source area that primarily delivered sedimentary detritus of this age to the Zacatecas Formation and from this in to the Nazas Formation.

The youngest recognised age population ranges from ~200–150 Ma (Early Jurassic–Late Jurassic). This age population makes up 11 % of 252 concordant zircon ages. Referring to recent literature (Barboza-Gudiño et al., 2008; Dickinson and Lawton, 2001; Lawton et al., 2010; Lawton and Molina Garza, 2014), the Nazas magmatic Arc is considered to be the most probable source area.

Taking the results of the U–Pb geochronology into account, the Zacatecas Formation and Nazas Formation sediments can be distinguished from the La Joya Formation sediments either due to the maximum depositional ages or on the basis of source area characteristics. The maximum depositional ages provided by the Zacatecas Formation samples range from Norian (Cha B9, RdC C4) to the Hettangian–Sinemurian boundary (RdC C6a). The dominant provenance areas of the Zacatecas Formation were most likely the Amazonian craton (~1780–1300 Ma), the Oaxaquia microcontinent (~1290–900 Ma) and Maya (Yucatan–Chiapas), blocks (~720–450 Ma) as well as the Permian–Triassic magmatic arc (~300–240 Ma). The Acatlán Complex and the Maya (Yucatan–Chiapas) block are likely source areas for ~445–310 Ma-old zircon grains. The source of the ~240–200 Ma-old detrital zircons is uncertain. It is notable, that the population ranging from ~445–310 Ma exclusively occurs in the Zacatecas Formation indicating that this source might have shut down in the Late Triassic. The population ranging from ~240–200 Ma is predominantly present in the Zacatecas Formation. However, the occurrence of this population in sample RdC C8 leads to the assumption that this source was active until at least the Pliensbachian. In addition to the discussed source areas of the samples Cha B9 and RdC C4, the sample RdC C6a contains two zircon grains providing Early Jurassic ages. Hence, the Zacatecas Formation contains either Upper Triassic or Lower Jurassic deposits. It is speculated that some of these deposits belong to the Lower Jurassic La Boca Formation. However, La Boca Formation is only present in the Sierra Madre Oriental (Fig. 3). Assigning these sediments to the La Boca Formation might either indicate the presence of La Boca Formation in the study areas (Mesa Central) or the presence of an alternative Lower Jurassic sediment source.

Sample LaB A3 provides an Oxfordian maximum depositional age for La Joya Formation. The Nazas arc evolved in an extensional regime with less erosion than the Andean-type Permian–Triassic arc (Stern and Dickinson, 2010). Most likely, the role of the Nazas arc as sediment source decreased with time. Hence, sample LaB A3 could be representative for a post-Nazas arc phase and received detritus from an unknown Late Jurassic source. However, since volcanic material is absent, sample LaB A3 could have received plutonic material from the Nazas arc because this sample has a high feldspar content and a similar heavy mineral assemblage as the samples with volcanic fragments. If the stratigraphic assignment of this sample to La Joya Formation is correct, it means that La Joya Formation is much younger than previously thought or, that in the locality La Ballena, the clastic sedimentation continues until the Oxfordian, as it happens in north-central Mexico with La Gloria Formation or as it has been previously described in some localities north of Charcas (Escalante-Martinez, 2006)

or in the Galeana area in Nuevo León (Pérez-Aguilar, 2018). The above is consistent with the significantly younger age suggested by Lawton and Amato (2017) for the Minas Viejas Formation wich overlying La Joya in the Sierra Madre Oriental.

The other La Joya Formation sediments provide maximum depositional ages from the Early Jurassic (RdC C8; Pliensbachian) to the Middle Jurassic (Cha B8; Aalenian, Cha B6; Callovian). The detritus of the samples Cha B6 and Cha B8 is dominated by material most likely derived from the Oaxaquia microcontinent (~1290–900 Ma), Maya (Yucatan–Chiapas), Chortis, Oaxaquia, Coahuila and Florida blocks (~720–450 Ma). Zircon ages ranging from ~200–150 Ma are indicative of detritus from the Nazas arc, which explains the volcanic fragments. However, characteristic ages for the Pan-African orogeny represented by the Maya (Yucatan–Chiapas), Chortis, Oaxaquia, Coahuila and Florida blocks are lacking in sample Cha B8. Additionally, the sample RdC C8 contains Permian–Triassic ages (~300–240 Ma) and Palaeoproterozoic–Middle Mesoproterozoic ages, indicative of detritus from the Amazonian craton (~1780–1300 Ma). Notably, Permian–Triassic ages are present within the Nazas Formation sediments (sample RdC C8) indicating exposure of this source until the Pliensbachian. Admittedly, the zircon abundances of the La Joya Formation samples are poorer compared to those of the Zacatecas and Nazas formations. According to Stern and Dickinson (2010), the Nazas arc is composed of volcanic rocks, which usually have lower zircon abundances than plutonic rocks (Permian–Triassic arc).

## 7. Conclusions

The main goal of this study was to identify similarities and differences among the Triassic and Jurassic siliciclastic sediments in the areas of La Ballena, Charcas and Real de Catorce in central Mexico. By means of a multi-method provenance analysis. The most important findings of this study are as followed:

- Sediment of Zacatecas, Nazas and La Joya formations is quartz rich with variable abundances of feldspar. Volcanic fragments are only present in the Nazas and La Joya formations.
- The sediments are characterized by low sediment recycling in the source area(s). Low Cr and Ni values exclude input from a mafic/ultramafic source.
- The most comoon translucent heavy minerals occurring in the samples are apatite and zircon. Apatite grains decrease from the southwest (La Ballena) towards the northeast (Real

de Catorce) either indicating stronger weathering conditions at Real de Catorce or a source area that delivered detritus exclusively to the the Real de Catorce locality.

- Zacatecas Formation sediments predominantly yielded Late Triassic or Early Jurassic maximum depositional ages (Norian–Hettangian/Sinemurian boundary), whereas La Joya Formation sediments yielded Early Jurassic–Middle Jurassic (Pliensbachian–Callovian) or Late Jurassic (Oxfordian) maximum depositional ages.
- Zacatecas and Nazas formation sediments received detritus possibly from the Amazonian craton (~1780–1300 Ma), the Oaxaquia microcontinent (~1290–900 Ma), the Maya (Yucatan–Chiapas), Chortis, Oaxaquia, Coahulia and Florida blocks (~720–450 Ma) and the Permian–Triassic magmatic arc (~300–240 Ma). The Acatlán Complex and the Maya (Yucatan–Chiapas) block were likely source areas for ~445–310 Ma-old zircon grains.
- Detrital zircon U–Pb ages in the Zacatecas Formation illustrate maximum depositional ages ranging from Norian (Late Triassic) to the Hettangian/Sinemurian boundary (Early Jurassic). The source of the ~240–200 Ma-old detrital zircons likely consisted of magmatic rocks related to the early disassambly of western Pangaea.
- La Joya Formation sediments received minor detritus from the Oaxaquia microcontinent (~1290–900 Ma), and the Maya (Yucatan–Chiapas), Chortis, Oaxaquia, Coahuila and Florida blocks (~720–450 Ma). Volcanic lithics were likely derived from the Nazas volcanic arc, as suggested by the presence of ~200–150 Ma-old detrital zircon grains.

**Acknowledgements**

Fieldwork for this research was funded by CONACyT (Consejo Nacional de Ciencia y tecnología) Grant: 169231. Funding was also provided by the Geologische Vereinigung (GV) through a Hans-Cloos-Prize to Guido Meinhold. Laboratory facilities at the Geoscience Center Göttingen and at the Geological Survey of Denmark and Greenland in Copenhagen are gratefully acknowledged. We thank Gerald Hartmann, Göttingen, for XRF analyses as well as comments and suggestions from Timothy F. Lawton and two other anonymous reviewers. This paper is published with the permission of the Geological Survey of Denmark and Greenland.

**Appendixes**

**Appendix 1. Sample preparation and analytical methods**

Thin section preparation followed standard techniques. For the purpose of different analysis, the samples were crushed with a hammer into fragments of approximately 0.5 cm. A part of the crushed material was further used to produce powder for the mounts for X-ray fluorescence (XRF) analysis. A planetary ball mill (Fritsch) was employed in order to receive the required grain size of <63 µm. The remaining crushed material was used to prepare the samples for the heavy mineral separation. A disc mill (Fritsch) was utilised to crush the sample material (~0.5 cm) into rock fragments <500 µm. Afterwards, the sample material was sieved (dry sieving) in order to obtain the desired grain fraction of 63–125 µm. The sample preparation including the planetary ball mill as well as the disc mill was conducted in the laboratories of the Department of Sedimentology and Environmental Geology of the University of Göttingen.

For whole-rock geochemical analysis, XRF sample mounts (40 mm in diameter) composed of 5.6 g Spectromelt, 2.8 g sample material (<63 µm) and 0.64 g lithium fluoride (LiF) were produced. An Autofluxer facility (Breitländer GmbH) was utilised to produce the XRF mounts by heating the sample powder up to 1250 °C. Shaking motions during the heating were necessary for homogenisation during the melting process. After heating, the melt was transferred into crucibles, composed of platinum, to cool for four minutes. The whole-rock geochemical analysis was carried out using a Panalytical AXIOSadvanced device. The sample preparation, production of the XRF mounts and the XRF analysis were conducted at the Department of Geochemistry of the University of Göttingen.

The Loss on Ignition (LOI) is a common technique to determine the abundances of carbon in samples. Analysis followed standard precedures by controlled heating (ignitation at 1000 °C) of dried samples.

Before operating the heavy mineral separation, the required grain fraction (63–125 µm) was treated with acetic acid ($CH_3COOH$) to remove carbonate from sample material. To separate the heavy minerals from the light minerals a heavy liquid (sodium polytungstate) with a density of approximately 2.87–2.88 g $cm^{-3}$ was used. The heavy minerals were distributed on an object slide and covered with a special resin with a light refraction of 1.662 (Cargille Meltmount™). A thin glass plate was used to cover the mixture of heavy minerals and resin. Finally, the object slide containing the heavy minerals and the resin was heated up to 70° C to ensure a sufficient embedding of the heavy minerals in the resin. The heavy mineral separation and production of the heavy mineral mounts was carried out in the heavy mineral laboratory of the Department of Sedimentology and Environmental Geology of the University of Göttingen.

For detrital zircon U-Pb geochronology, zircon grains were separated from the remaining heavy mineral concentrates using a Frantz magnetic separator to remove the magnetic minerals. From the nonmagnetic fraction, the zircon grains were picked by hand under a binocular microscope (Olympus SZX7) and placed on double-side adhesive tape and embedded in epoxy resin. The next step included the grinding and polishing of the mount to ensure smooth surfaces of the zircons and to remove scratches on the mount surface. Therefore, a Metaserv 2000 Grinder/Polisher (Buehler) machine was used. The whole process was carried out in the heavy mineral laboratory of the Department of Sedimentology and Environmental Geology of the University of Göttingen. Finally, the mount was scanned by cathodoluminescence (CL) employing a JEOL JXA 8900 RL (JEOL/Japan) electron microprobe in the Department of Geochemistry of the University of Göttingen. CL imaging allows visualisation of the internal structure of the zircon grains chosen for U–Pb geochronology.

Seven samples were used for detrital zircon U–Pb geochronology (Tables S7 to S13. One sample from La Ballena (LaB A3), three samples from Charcas (Cha B6, Cha B8, Cha B9) and three samples from Real de Catorce (RdC C4, RdC C6a, RdC C8) were analyzed. The samples were chosen with the intention to represent each profile from the bottom to the top. The U–Pb geochronology was performed at the Geological Survey of Denmark and Greenland (GEUS) in Copenhagen employing a New Wave 213 nm Nd: YAG laser ablation (LA) system coupled to a Thermo-Fisher Scientific Element 2 SF-ICPMS (Meinhold and Frei, 2008; Frei and Gerdes, 2009). To remove surface lead contamination, the zircon mount was cleaned in an ultrasonic bath before placing it into the sample cell. The laser run with a repetition rate of 10 Hz and a laser fluency on the sample of 10 J $cm^{-2}$. During the measurement, two different standards including the GJ1 zircon as well as the Plešovice standard zircon were utilised. All data were acquired with single-spot analysis. With the exception of sample LaB A3 (20 µm) a laser beam size of 25 µm was employed. The total time for each measurement was 80 seconds (30 seconds background, 30 seconds signal (ablation), 20 seconds washout). The instrument was tuned to achieve large and stable signals for the $^{206}Pb$ and $^{238}U$ peaks, low background count rates and low oxide production rates (<0.8 %). During the measurement the following isotopes were measured: $^{202}Hg$, $^{204}(Pb + Hg)$, $^{206}Pb$, $^{207}Pb$, $^{208}Pb$, $^{232}Th$ and $^{238}U$. The final data reduction was carried out through the software Iolite (Paton et al., 2011) using the integrated DRS routine VizualAge (Petrus and Kamber, 2012).

The common Pb corrected data were plotted in histograms, concordia diagrams (only LaB A3) and probability density curves to clarify the occurring age populations. Isoplot (Ludwig, 2003) and DensityPlotter v2.2 (Vermeesch, 2012) were employed to compile the illustrations. The resulting $^{206}Pb/^{238}U$ ages were used to illustrate zircon ages ≤800 Ma. The $^{206}Pb/^{207}Pb$ ages were used to depict older zircon ages. Analysis within a 95–105 % concordance level, are considered to be concordant. Furthermore, analysis illustrating a discordance >10 % were rejected from the data set and not used for the interpretation. The geological time scale provided by the Gradstein et al. (2012) was used as reference. Uncertainties in ages are quoted at the 2-sigma (95 % confidence) level. Meinhold et al. (2010) who presented U–Pb dates on zircon grains previously dated by SHRIMP-II have tested the accuracy and reproducibility of the applied LA-ICPMS method. Furthermore, chips of the TEMORA 1 zircon standard were treated as unknown during the LA-ICPMS analytical session by Meinhold et al. (2010).

**Appendix 2. Petrography**

Sample LaB A3 is a moderate sorted, medium-grained to coarse-grained sandstone that provides grain sizes ranging from 0.29 to 0.71 mm. However, a very few grains can be characterized as fine-grained. The majority of the grains provide subrounded to subangular grain shapes. Furthermore, grain contacts are obvious and fine cement between the grains is detectable. Overall, 320 grains were counted and the main components are quartz (46.56 %), feldspar (30 %) and lithic fragments (23.44 %). Remarkably, very high feldspar and chert (Lm) contents in comparison to the remaining samples without volcanic fragments can be recognised. However, most of the feldspar grains are highly affected by alteration, which might be a possible explanation for the fine-grained cement occurring between the grains. Sample LaB A3 reveals the third highest $Na_2O$ concentration among all samples. This observation is consistent with the high feldspar content. The QFL analysis yields a magmatic arc as a possible provenance.

Sample Cha B2 is a very fine-grained siltstone that provides grain sizes <0.008 mm. However, this sample illustrates graded bedding.

Sample Cha B3 is a medium-grained to coarse-grained siltstone that provides grain sizes ranging from 0.017 to 0.04 mm and shows signs of weathering. Besides clay minerals and quartz, this sample contains calcite. About 7.6 wt% CaO and an elevated LOI are in consistency with the calcite abundance.

Sample Cha B4 is a well-sorted, fine-grained sandstone that provides grain sizes ranging from 0.17 to 0.25 mm. The majority of the grains are subrounded to subangular. Overall, 314 grains were counted and the main components are quartz (92.36 %), feldspar (3.5 %) and lithic fragments (4.14 %). In this sample, it is difficult to distinguish between cement and matrix because in a very few cases grain contacts are obvious. However, fine-grained material can be recognised between the grains. High abundances of calcite are consistent with elevated values for CaO and LOI. Calcite predominately occurs as cement or matrix. However, single calcite grains were also recognised. The QFL analysis yields a recycled orogen as a possible source area.

Sample Cha B5 is a coarse-grained siltstone to fine-grained sandstone that provides grain sizes ranging from 0.05 to 0.12 mm. The grains are predominantly subangular to angular. The major components are quartz (93.67 %), feldspar (2.71 %) and lithic fragments (3.61 %). Both, plagioclase and K-feldspar grains were recognised. However, the most frequent variety occurring in this sample is K-feldspar. Observed high abundances of calcite are consistent with elevated values for CaO and LOI. Grain contacts are obvious but calcite often occurs as cement. Furthermore, the thin section provides areas where calcite illustrates greater abundances compared to other areas in this sample. The QFL analysis yields a recycled orogen as a possible provenance area for this sample.

Sample Cha B9 is a moderate sorted, fine-grained to medium-grained sandstone that provides grain sizes ranging from 0.17 to 0.34 mm. The grains are mostly subrounded to angular. Grain contacts and very fine cement between the grains are recognisable. In a very few cases muscovite occurs in this sample. Remarkably, Cha B9 does not contain calcite. Overall, 309 grains were counted. The major components are quartz (95.05 %), feldspar (3.51 %) and lithic fragments (1.55 %). The QFL analysis yields a continental block as a possible source area. However, this sample plots very close to the field of a recycled orogen.

Sample RdC C1 is a very fine-grained siltstone highly affected by alteration. Further differentiation is not possible.

Sample RdC C2 is a poorly-sorted, medium-grained to very coarse-grained sandstone that provides grain sizes ranging from 0.3 to 1.5 mm. The majority of the grains are subangular to angular. Fine-grained cement between the grains and a couple of muscovite grains are recognisable. Overall, 429 grains were counted. The major components are quartz (89.98 %), feldspar (1.63 %) and lithic fragments (8.39 %). In contrast to the remaining samples without volcanic fragments sample RdC C2 predominately consists of polycrystalline

quartz. Furthermore, sample RdC C2 reveals the second highest chert content (Lm) (Table 2). The QFL analysis yields a recycled orogen as a possible source area.

Sample RdC C3 is a well-sorted, medium-grained sandstone that provides grain sizes ranging from 0.3 to 0.49 mm. The grains are mostly subangular. The sample can be characterized due to a minor occurrence of quartz, feldspar and lithic fragments. One of the main components is calcite, which is consistent with a high CaO content (7.93 wt%) and an elevated LOI. Remarkably, a large amount of dolomite is consistent with the highest MgO concentration (6.31 wt%) among all analyzed samples.

Sample RdC C4 is a moderately sorted, very fine-grained to medium-grained sandstone that illustrates stratification. The thin section can be divided into three areas. The first area is dominated by subrounded to subangular grains that provide grain sizes ranging from 0.07 to 0.15 mm. Grain contacts and fine cement between the grains are obvious. A very few muscovite grains were recognised in the cement. The second area is composed of fine-grained to medium-grained, subrounded to subangular grains with grain sizes ranging from 0.24 to 0.29 mm. The fine cement between the grains does not contain muscovite. The third area mostly consists of angular grains, which are medium-grained. Grain sizes range from 0.27 to 0.39 mm. The abundance of fine cement decreases resulting in an increase of grain contacts. Furthermore, this area is composed of less chert and polycrystalline quartz compared to the finer areas. Overall, 400 grains were counted and the major components are quartz (94.5 %), feldspar (1.25 %) and lithic fragments (4.25 %). The QFL analysis yields a recycled orogen as a possible provenance area.

Sample RdC C6 is a coarse-grained siltstone with grain sizes ranging from 0.03 to 0.5 mm. The grains are predominantly subrounded to subangular. The major component is a fine-grained matrix including monocrystalline quartz, polycrystalline quartz and feldspar in minor abundances. However, due to the thin section observations, this sample could also be characterized as a wacke with a major portion of matrix and a minor portion of rock building fragments.

Sample RdC C6a is a poorly sorted, fine-grained to coarse-grained quartzite with grain sizes ranging from 0.08 to 0.5 mm. The components mostly provide angular grain shapes. Quartz cement occurs between the grains. Overall, 400 grains were counted and the major components are quartz (95 %) and lithic fragments (5 %). The QFL analysis yields a recycled orogen as a possible source area.

Sample RdC C10 is a well-sorted, very fine-grained to fine-grained sandstone that provides grain sizes ranging from 0.07 to 0.2 mm. The grains are mostly subrounded to

angular. Fine cement between the grains, most likely composed of clay, can be recognised. Overall, 465 grains were counted and the major components are quartz (93.12 %), feldspar (2.37 %) and lithic fragments (4.52 %). The QFL analysis yields a recycled orogen as a possible provenance area.

Sample RdC C14 is a coarse-grained siltstone with grain sizes ranging from 0.04 to 0.65 mm. The grains are predominately subangular to angluar. The major component is a fine-grained matrix including monocrystalline quartz as well as polycrystalline quartz in minor abundances. However, due to the thin section observations, this sample could also be characterized as a wacke with a major portion of matrix and a minor portion of rock building fragments.

Sample LaB A1 is a well-sorted, very coarse-grained sandstone to conglomeratic rock that provides grain sizes ranging from 1.5 to 3 mm. The majority of the grains are subrounded. However, the polycrystalline quartz grains even illustrate well rounded grain shapes. Furthermore, only very small parts of this thin section provide cement between the grains. The main part can be characterized due to a lack of matrix or cement. Overall, 311 grains were counted including quartz (55.95 %), feldspar (9.65 %) and lithic fragments (34.4 %). The volcanic fragments include well developed plagioclase laths without a preferred orientation. They make up 56.1 % of the lithic fragments, whereas chert contributes 43.9 %. The QFL analysis yields a recycled orogen as a possible source area.

Sample Cha B6 is a moderate sorted, fine-grained to medium-grained sandstone that provides grain sizes ranging from 0.24 to 0.49 mm. The grains are subrounded to angular. The majority of the polycrystalline quartz grains provide rounded grains. Grain contacts are obvious but calcite occurs only irregular between the grains. Fine-grained cement only appears in certain parts of the thin section. Overall, 345 grains were counted and the major components are quartz (38.26 %), feldspar (32.75 %) and lithic fragments (28.99 %). The high feldspar content is consistent with a $Na_2O$ concentration of 3.85 wt%. Remarkably, sample Cha B6 illustrates the highest feldspar and the lowest quartz content within the samples with volcanic fragments. Volcanic fragments imply plagioclase laths without a preferred orientation. Due to a lack of chert (Lm), volcanic fragments make up 100 % of the lithic fragments. The plagioclase laths are predominately small. The QFL analysis yields a magmatic arc as a possible provenance area.

Sample Cha B7 is a polymictic conglomeratic rock that provides grain sizes in the array of very fine pebbles (2.8 to 3.4 mm). The majority of the grains are rounded to subangular. However, the monocrystalline quartz grains also provide well rounded grain

shapes and illustrate different grain sizes. The grains are embedded in a fine matrix or cement most likely composed of clay minerals. Distinguishing between matrix and cement is difficult in this sample. Overall, 344 grains were counted and the major components are quartz (82.58 %), feldspar (9.88 %) as well as lithic fragments (7.56 %). The majority of the feldspar grains are extremely affected by alteration. Due to low abundances of volcanic fragments and chert, the appearance of lithic fragments is scarce in this sample. Volcanic fragments imply small plagioclase laths and make up 80.8 % of lithic fragments, whereas chert contributes only 19.2 %. Nevertheless, the quartz content is the highest within the samples with volcanic fragments. The QFL analysis yields a recycled orogen as a possible source area. However, the sample plots very close to the field representing a continental block provenance.

Sample Cha B8 is a moderate sorted, fine-grained to medium-grained sandstone that provides grain sizes ranging from 0.17 to 0.39 mm. The grains are predominately rounded to subangular. Slight amounts of clay minerals make up the cement between the grains. Overall, 354 grains were counted and the major components are quartz (79.94 %), feldspar (5.93 %) and lithic fragments (14.12 %). The sample can be characterized due to a high content of quartz and the lowest feldspar content within the samples with volcanic fragments. The feldspar grains are mainly plagioclase. The volcanic fragments contain very small plagioclase laths. Volcanic fragments make up 86 % of the lithic fragments, whereas chert contributes 14 %. The QFL analysis yields a recycled orogen as a possible provenance area.

Sample Cha B10 is a poorly sorted, fine-grained to coarse-grained sandstone that provides grain sizes ranging from 0.15 to 0.6 mm. The grains are mostly rounded to subangular. Especially, the monocrystalline quartz reveals rounded grains. Grain contacts occur in great amounts and fine cement can be recognised between the grains. Furthermore, minor abundances of calcite reside between the grains. The cement is most likely composed of clay minerals. Overall, 453 grains were counted. The sample consists of quartz (58.5 %), feldspar (19.65 %) and lithic fragments (21.85 %). The sample is characterized by the second highest feldspar content among all samples with volcanic fragments, which is consistent with a $Na_2O$ concentration of 4.33 wt%. The volcanic fragments make up 88.8 % of the lithic fragments, whereas chert contributes only 11.2 %. The plagioclases within the volcanic fragments occur as well developed laths. Feldspar grains are mainly represented by plagioclase. The QFL analysis yields a recycled orogen as a possible source area.

Sample Cha B11 is a moderate sorted, fine-grained to medium-grained sandstone that provides grain sizes ranging from 0.16 to 0.43 mm. The grains are predominately subrounded to subangular. Unlike to the majority of the analyzed samples, this sample does not provide

calcite between the grains. Cement only occurs in certain areas of the thin section and makes up a minor portion. Overall, 387 grains were counted and the major components are quartz (59.43 %), feldspar (19.38 %) and lithic fragments (21.19 %). The high feldspar content is consistent with a $Na_2O$ concentration of 4.29 wt%. The volcanic fragments illustrate well developed plagioclase laths and constitute 87.8 % of the lithic fragments, whereas chert contributes only 12.2 %. The feldspar content can be characterized by approximately similar abundances of plagioclase and K-feldspar. The QFL analysis yields a recycled orogen as a possible provenance area. Samples Cha B10 and Cha B11 provide very similar abundances of the mineral components. However, sample Cha B11 is more fine-grained and provides greater amounts of poorly rounded grains than sample Cha B10.

Sample RdC C8 is well-sorted, fine-grained sandstone that provides grains sizes ranging from 0.15 to 0.17 mm. During the fieldwork, this sample was identified as pyroclastic deposit. However, according to the thin section analysis, this sample is likely of sedimentary origin. Interestingly, sample RdC C8 is extremely affected by weathering, inasmuch as the volcanic fragments are completely altered. Due to the high degree of weathering, this sample was not considered for mineral counting.

Sample RdC C11 is a polymictic conglomeratic rock that provides grains sizes ranging from 0.24 to 2.8 mm. The grains are rounded to subangular. Furthermore, they are embedded in a fine-grained cement. The volcanic fragments within this sample contain well developed plagioclase laths without preferred orientation. Overall, 396 grains were counted and the major components are quartz (75.26 %), feldspar (8.08 %) and lithic fragments (16.67 %). The volcanic fragments make up 69.7 % of the lithic fragments, whereas chert contributes 30.3 %. The QFL analysis yields a recycled orogen as a possible source area.

Sample RdC C12 is a poorly sorted, very fine-grained to medium-grained sandstone that provides grain sizes ranging from 0.08 to 0.26 mm. The majority of the grains illustrate subangular to angular grain shapes. The grains are embedded in fine cement. However, cement occurs in slight abundances because strong grain contacts are recognisable. Remarkably, chert is lacking in this sample, so that volcanic fragments make up 100 % of the lithic fragments. The volcanic fragments contain very small plagioclase laths without preferred orientation. K-feldspar is the dominant feldspar phase. Small abundances of chlorite (~2–3 %) appear in this sample. Overall, 330 grains were counted and the major components are quartz (82.42 %), feldspar (9.7 %) and lithic fragments (7.88 %). The QFL analysis yields a recycled orogen as a possible source area.

Sample RdC C13 is a well sorted, very fine-grained to fine-grained sandstone that provides grain sizes ranging from 0.11 to 0.21 mm. The grains are predominantly subrounded to angular. In contrast to the previous sample, chlorite is lacking and clay cement occurs in high abundances between the grains. The sample is highly affected by weathering and the dark yellow to brown areas might be remnants of volcanic fragments. However, the majority of the volcanic fragments within this sample are not affected by weathering. The plagioclase laths within the volcanic fragments are small. Overall, 387 grains were counted. The sample is composed of quartz (69.21 %), feldspar (10.48 %) and lithic fragments (20.32 %). Similar to the previous sample chert is lacking and volcanic fragments make up 100 % of the lithic fragments. The QFL analysis yields a recycled orogen as a possible source area.

**References**


Armstrong-Altrin, J.S., and Verma, S.P., 2005, Critical evaluation of six tectonic setting discrimination diagrams using geochemical data of Neogene sediments from known tectonic settings: Sedimentary Geology, v. 177, p. 115–129.

Barboza-Gudiño, J.R., Hoppe, M., Gómez-Anguiano, M., and Martínez-Macías, P.R., 2004, Aportaciones para la interpretación estratigráfi ca y estructural de la porción noroccidental de la Sierra de Catorce, San Luis Potosí, México: Revista Mexicana de Ciencias Geológicas, v. 21, p. 299–319.

Barboza-Gudiño, J.R., Orozco-Esquivel, M.T., Gómez-Anguiano, M., and Zavala-Monsiváis, A., 2008, The early Mesozoic volcanic arc of western North America in northeastern Mexico. Journal of South American Earth Sciences, v. 25, p. 49–63.

Barboza-Gudiño, J.R., Zavala-Monsiváis, A., Venegas-Rodríguez, G., and Barajas-Nigoche, L.D., 2010, Late Triassic stratigraphy and facies from northeastern Mexico: Tectonic setting and provenance: Geosphere, v. 6, p. 621–640.

Barboza-Gudiño, J.R., 2012. Sedimentary Tectonics and Stratigraphy: The Early Mesozoic Record in Central to Northeastern Mexico, *in* Elitok, Ö., ed., Stratigraphic Analysis of Layered Deposits: http://www.intechopen.com/books/stratigraphicanalysis-of-layered-deposits/sedimentary-tectonics-and-straigraphy-the-early-mesozoicrecord-in-central-to-northeastern-mexico.

Barboza-Gudiño, J.R., Ocampo-Díaz Y.Z. E., Zavala-Monsiváis, A., López-Doncel, R.A., 2014, Procedencia como herramienta para la subdivisión estratigráfica del Mesozoico

temprano en el noreste de México: Revista Mexicana de Ciencias Geológicas, v. 31, núm. 3, p. 303-324.

Blickwede, J.F., 2001, The Nazas Formation: A detailed look at the early Mesozoic convergent margin along the western rim of the Gulf of Mexico Basin, *in* Bartolini C., Buffler, R.T., and Cantu-Chapa, A., eds., The Western Gulf of Mexico Basin: Tectonics, Sedimentary Basins and Petroleum Systems: American Association of Petroleum Geologists Memoir, v. 75, p. 317–342.

Burckhardt, C., and Scalia, S., 1905, La faune marine du Trias Supérieur de Zacatecas. Instituto de Geología de México Boletín, v. 21, 44 p.

Cawood, P. A., Hawkesworth, C.J., and Dhuime, B., 2012, Detrital zircon record and tectonic setting: Geology, v. 40, p. 875-878, doi:810.1130/G32945.32941.

Centeno-García, E., 2005, Review of Upper Paleozoic and Lower Mesozoic stratigraphy and depositional environments of central and west Mexico: Constraints on terrane analysis and paleogeography, *in* Anderson, T.H., Nourse, J.A., McKee, J.W., and Steiner, M.B., eds., The Mojave-Sonora Megashear Hypothesis: Development, Assessment, and Alternatives: Geological Society of America Special Paper, v. 393, p. 233–258.

Dickinson, W.R., 1981, Plate tectonic evolution of the Southern Cordillera: *in* Dickinson, W.R., and Payne, W.D., eds., Relations of tectonics to ore deposits in the Southern Cordillera: Arizona Geological Society Digest, v. 14, p. 113–135.

Dickinson, W.R., and Lawton, T.F., 2001, Carboniferous to Cretaceous assembly and fragmentation of Mexico. Geological Society of America Bulletin, v. 113, p. 1142–1160.

Dickinson, W.R., and Gehrels, G.E., 2009, Use of U–Pb ages of detrital zircons to infer maximum depositional ages of strata: A test against a Colorado Plateau Mesozoic database: Earth and Planetary Science Letters, v. 288, p. 115–125.

Dott, R.H. Jr., 1964, Wacke, greywacke and Matrix–what approach to immature sandstone classification? Journal of Sedimentary Petrology, v. 34, p. 625–632.

Eguiluz-de Antuñano, S., Aranda-García M., Buitrón-Sánchez, B. E., 2014, The Gran Tesoro and Nazas Formations: Evolution of the Upper Triassic-Lower Jurassic sequences in Mexico and their tectogenic significance, Boletín de la Sociedad Geológica Mexicana, v. 66, p. 507-539.

English, J.M., and Johnston, S., 2004, The Laramide Orogeny: What Were the Driving Forces? International Geology Review, v. 46, p. 833–838.

Escalante-Martínez, J. L., 2006, Análisis estructural de los afloramientos de la secuencia siliciclástica marina del Triásico Superior en el área de Presa de Santa Gertrudis, S. L.

P". Facultad de Ingeniería, Área de Ciencias de la Tierra UASLP, 123 p.

Fedo, C.M., Sircombe K.N., and Rainbird, R.H. 2003, Detrital zircon analysis of the sedimentary record. *in* Hanchar, J.M., and Hoskin, P.O., eds., Zircon: Experiments, Isotopes and Trace Element Investigations: Mineralogical Society of America, Reviews in Mineralogy, v. 53, p. 277–303.

Fitz-Díaz, E., Lawton, T., Juarez, E., Chavez-Cabello, G., 2017, The Cretaceous-Paleogene Mexican orogene: Structure, basin development, magmatism and tectonics, Earth-Science Reviews, DOI·10.1016/j.earscirev.2017.03.002

Floyd, P.A., and Leveridge, B.E., 1987, Tectonic environment of Devonian Gramscatho basin, south Cornwall: framework mode and geochemical evidence from turbiditic sandstones: Journal of the Geological Society, London, v. 144, p. 531–542.

Frei, D., Gerdes, A., 2009. Precise and accurate in-situ U–Pb dating of zircon with high sample throughput by automated LA-SF-ICP-MS. Chemical Geology 261, 261–270.

Garver, J.I., Royce, P.R., Smick, T.A., 1996. Chromium and nickel in shale of the Taconic foreland: a case study for the provenance of fine-grained sediments with an ultramafic source. Journal of Sedimentary Research 66, 100–106.

Goldhammer, R.K., Lehmann, P.J., Todd, R.G., Wilson, J.L., Ward, W.C., and Johnson, C.R., 1991, Sequence stratigraphy and cyclostratigraphy of the Mesozoic of the Sierra Madre Oriental, northeast Mexico, a field guidebook: Gulf Coast Section, Society of Economic Paleontologists and Mineralogists, 85 p.

Goldhammer, R.K., 1999, Mesozoic sequence stratigraphy and sedimentary evolution of northeast Mexico. *in* Bartolini, C., Wilson, J.L., and Lawton, T.F., eds., Mesozoic Sedimentary and Tectonic History of North-Central Mexico: Geological Society of America Special Paper, v. 340, p. 1–58.

Gradstein, F.M., Ogg, J.G., and Schmitz, M.D., 2012, The Geologic Time Scale 2012: Boston, Elsevier, 1176 p.

Hoppe, M., 2000, Geologische Kartierung (1:10 000) im Gebiet Ojo de Agua, nordwestliche Sierra de Catorce und sedimentpetrologische Untersuchungen an präoberjurassischen Sedimenten ("Zacatecas Formation") [M.S. thesis]: Clausthal, Technische Universität Clausthal.

Hubert, J.F., 1962, A zircon-tourmaline-rutile maturity index and the interdependence of the composition of heavy mineral assemblages with the gross composition and texture of sandstones: Journal of Sedimentary Petrology, v. 32, p. 440–450.

Imlay, R.W., Cepeda, E., Álvarez, M. Jr., and Diaz, T., 1948, Stratigraphic relations of certain Jurassic formations in eastern Mexico: American Association of Petroleum Geologists Bulletin, v. 32, p. 1750-1761.

Johnson, C.A., 1989, Structural analysis of the fold and thrust belt in the vicinity of Monterrey, northeastern Mexico: Houston Texas, Exxon Production Research Company Report (unpublished).

Keppie, J.D., Dostal, J., Cameron, K.L., Solari, L.A., Ortega- Gutiérrez, F., and Lopez, R., 2003, Geochronology and geochemistry of Grenvillian igneous suites in the northern Oaxacan Complex, southern Mexico: Tectonic implications: Precambrian Research, v. 120, p. 365–389.

La Bas, M.J., and Streckeisen, A.L., 1991, The IUGS systematics of igneous rocks: Journal of the Geological Society London, v. 148, p. 825–835.

Lawton, T. F., and Amato, J. M., 2017, U-Pb ages of salt diapir xenoliths, La Popa basin: Implications for salt age in onshore Mexico salt basins: Lithosphere, v. 9, p. 745-758, https://doi.org/710.1130/L1658.1131.

Lawton, T.F., Molina-Garza, R.S., 2014. U–Pb geochronology of the type Nazas Formation and superjacent strata, northeastern Durango, Mexico: Implications of a Jurassic age for continental-arc magmatism in north-central Mexico. Geological Society of America Bulletin, doi: 10.1130/B30827.1

Lawton, T.F., Barboza-Gudiño, R., González-León, C.M., Gray, G.G., Iriondo, A., Leggett, W.J., Peryam, T.C., and Rubio-Cisneros, I.I., 2010, Latest Triassic-Middle Jurassic Age of Cordilleran Nazas arc in Mexico indicated by U–Pb detrital zircon and volcanic-rock ages: Geological Society of America, Abstracts with Programs, v. 42, p. 345.

Ludwig, K.R., 2003, Isoplot/Ex 3.00: A Geochronological Toolkit for Microsoft Excel: Berkeley Geochronology Center, Special Publication, v. 4, p. 1–70.

Mange, M.A. and Maurer, H.F.W. (1992) Heavy Minerals in Colour. Chapman and Hall, London, 147. http://dx.doi.org/10.1007/978-94-011-2308-2

Martens, U., Weber, B., and Valencia, V.A. 2010, U–Pb geochronology of Devonian and older Paleozoic beds in the southwestern Maya Block, Central America: its affinity with Peri-Gondwanan terranes: Geological Society of America Bulletin, v. 122, p. 815–829.

Martini, M., Ortega-Gutierrez, F., 2016, Tectono-stratigraphic evolution of eastern Mexico during de break-up of Pangea: A review, Earth Sci. Rev. http:/dx.doi.org/10.1016/j.earscirev.2016.06.013

Marton, G., and Buffler, R.T. 1994, Jurassic reconstruction of the Gulf of Mexico Basin: International Geology Review, v. 36, p. 545–586.

McLennan, S.M., Hemming, S., McDaniel, D.K., and Hanson, G.N., 1993, Geochemical approaches to sedimentation, provenance and tectonics, *in* Johnsson, M.J., and Basu, A., eds., Processes Controlling the Composition of Clastic Sediments: Geological Society of America Special Paper, v. 284, p. 21–40.

Meinhold, G., 2010. Rutile and its applications in earth sciences. Earth-Science Reviews, 102, 1–28.

Meinhold, G., Frei, D., 2008. Detrital zircon ages from the islands of Inousses and Psara, Aegean Sea, Greece: constraints on depositional age and provenance. Geological Magazine, 145, 886–891.

Meinhold, G., Kostonpoulos, D., and Reischmann, T., 2007, Geochemical constraints on the provenance and depositional setting of sedimentary rocks from the island of Chios, Inousses, Psara, Aegean Sea, Greece: implications for the evolution of Palaeotethys: Journal of the Geological Society London, v. 164, p. 1145–1163.

Meinhold, G., Reischmann, T., Kostopoulos, D., Lehnert, O., Matukov, D., and Sergeev, S., 2008, Provenance of sediments during subduction of Palaeotethys: detrital zircon ages and olistolith analysis in Palaeozoic sediments from Chios Island, Greece: Palaeogeography, Palaeoclimatology, Palaeoecology, v. 263, p. 71–91.

Meinhold, G., Kostopoulos, D., Reischmann, T., Frei, D., BouDagher-Fadel, M.K., 2009. Geochemistry, provenance and stratigraphic age of metasedimentary rocks from the eastern Vardar suture zone, northern Greece. Palaeogeography, Palaeoclimatology, Palaeoecology, 277, 199–225.

Meinhold, G., Reischmann, T., Kostopoulos, D., Frei, D., Larionov, A.N., 2010. Mineral chemical and geochronological constraints on the age and provenance of the eastern Circum-Rhodope Belt low-grade metasedimentary rocks, NE Greece. Sedimentary Geology, 229, 207–223.

Michalzik, D., 1991, Facies sequence of Triassic-Jurassic red beds in the Sierra Madre Oriental (NE Mexico) and its relation to the early opening of the Gulf of Mexico: Sedimentary Geology, v. 71, p. 243–259.

Mixon, R.B., Murray, G.E., and Diaz, T.G., 1959, Age and correlation of Huizachal Group (Mesozoic), state of Tamaulipas, Mexico: American Association of Petroleum Geologists Bulletin, v. 43, p. 757–771.

Molina-Garza, R.S., 2005, Paleomagnetic reconstruction of Coahuila, Mexico: The Late Triassic Acatita intrusives: Geofísica Internacional, v. 44, p. 197–210.

Morton, A.C., 1984, Stability of detrital heavy minerals in Tertiary sandstones of the North Sea Basin: Clay Minerals, v. 19, p. 287–308.

Morton, A.C., 1986, Dissolution of apatite in North Sea Jurassic sandstones: implications for the generation of secondary porosity: Clay Minerals, v. 21, p. 711–733.

Morton, A.C., 2012, Value of heavy minerals in sediments and sedimentary rocks for provenance, transport history and stratigraphic correlation, *in* Sylvester, P., ed.,. Quantitative mineralogy and microanalysis of sediments and sedimentary rocks: Mineralogical Association of Canada Short Course Series, v. 42, p. 133–165.

Morton, A.C., and Hallsworth, C.R., 1994, Identifying provenance specific features of detrital heavy mineral assemblages in sandstones: Sedimentary Geology, v. 90, p. 241–256.

Morton, A.C., and Hallsworth, C.R., 1999, Processes controlling the composition of heavy mineral assemblages in sandstones: Sedimentary Geology, v. 124, p. 3–29.

Morton, A.C., Whitham, A.G., and Fanning, C.M., 2005, Provenance of Late Cretaceous to Paleocene submarine fan sandstones in the Norwegian Sea: Integration of heavy mineral, mineral chemical and zircon age data: Sedimentary Geology, v. 182, p. 3–28.

Morton, A.C., and Hallsworth, C.R., 2007, Stability of detrital heavy minerals during burial diagenesis. *in* Mange, M., and Wright, D.K., eds., Heavy Minerals In Use. Developments in Sedimentology, v. 58, p. 215–245.

Murphy, J.B., Pisarevsky, S.A., Nance, R.D., and Keppie, J.D., 2004, Neoproterozoic–Early Paleozoic evolution of peri Gondwanan terranes: Implications for Laurentia-Gondwana connections: International Journal of Earth Sciences, v. 93, p. 659–682.

Nance, R.D., Keppie, J.D., Miller, B.V., Murphy, J.B., and Dostal, J., 2009, Palaeozoic palaeogeography of Mexico: Constraints from detrital zircon age data, *in* Murphy, J.B., Keppie, J.D., and Hynes, A.J., eds., Ancient orogens and modern analogues: Geological Society of London Special Publication, v. 327, p. 239–269.

Ortega-Flores, B., Solari, L., Lawton, F.T., and Ortega-Obregón, C., 2014, Detrital-zircon record of major Middle Triassic–Early Cretaceous provenance shift, central Mexico: demise of Gondwanan continental fluvial systmes and onset of back-arc volcanism and sedimentation: International Geology Review, v. 56, p. 237–261.

Pantoja-Alor, J., 1972, La Formación Nazas del Levantamiento de Villa Juárez, Estado de Durango: Memorias de la Segunda Convención Nacional de la Sociedad Geológica Mexicana, p. 25–31.

Paton, C., Hellstrom, J., Paul, B., Woodhead, J., and Hergt, J., 2011, Iolite: Freeware for the visualisation and processing of mass spectrometric data: Journal of Analytical Atomic Spectrometry, v. 26, p. 2508–2518.

Pearce, J.A., 1996, A user´s guide to basalt discrimination diagrams, *in* Wyman, D.A., ed., Trace element geochemistry of Volcanic rocks: Applications for Massive Sulphides Exploration: Geological Association of Canada, Short Course Notes, v. 12, p. 79–113.

Pérez-Aguilar J. F., 2018, Correlación estratigráfica de la Formación La Joya del Jurásico Medio en la zona de Galeana, Nuevo León y la Sierra de Catorce, San Luis Potosí, Tesis, Ingeniro en Geología, Universidad Autónoma de San Luis Potosí, 114 p.

Pérez-Casillas, I. G., 2018, Sedimentación y evolución tectónica de la Cuenca de Catorce, Jurásico Medio de la Mesa Central de México, M. C., tesis, Universidad Autónoma de San Luis Potosí, 101 p.

Pettijohn, F.J., 1941, Persistence of heavy minerals and geologic age: Journal of Geology, v. 49, p. 610–625.

Petrus, J.A., and Kamber, B.S., 2012, VizualAge: A Novel Approach to Laser Ablation ICP-MS U–Pb Geochronology Data Reduction: Geostandards and Geoanalytical Research, v. 36, p. 247–270.

Pindell, J.L., Dewey, J.F., 1982, Permo-Triassic reconstruction of western Pangea and the evolution of the Gulf of Mexico/Caribbean region, Tectonics 1, 179-211.

Pindell, J.L., Kennan, L., 2009, Tectonic evolution of the Gulf of Mexico, Caribbean and northern South America in the mantle reference frame: an update, Geol. Soc. Lond. Spec. Publ. 328, 1-55.

Rino, S., Kon, Y., Sato, W., Maruyama, S., Santosh, M., and Zhao, D., 2008, The Grenvillian and Pan-African orogens: World's largest orogenies through geologic time and their implications on the origin of superplume: Gondwana Research, v. 14, p. 51–72.

Rubatto, D., 2002, Zircon trace element geochemistry: partitioning with garnet and the link between U–Pb ages and metamorphism: Chemical Geology, v. 184, p. 123–138.

Rollinson, H.R., 1993, Using geochemical data: evaluation, presentation, interpretation: Logman, London, 352 p.

Rubio-Cisneros, I.I., and Lawton, T.F., 2011, Detrital zircon U–Pb ages of sandstones in continental red beds at Valle de Huizachal, Tamaulipas, NE Mexico: Record of Early–Middle Jurassic arc volcanism and transition to crustal extension: Geosphere, v. 7, p. 159–170.

Rudnick, R.L., and Gao, S., 2003, Composition of the Continental Crust: Treatise on Geochemistry, v. 3, p. 1–64.

Sedlock, R.L., Ortega-Gutiérrez, F., and Speed, R.C., 1993, Tectonostratigraphic terranes and tectonic evolution of Mexico: Geological Society of America Special Paper, v. 278, p. 153.

Steiner, M.B., and Walker, J.D., 1996, Late Silurian plutons in Yucatan: Journal of Geophysical Research, v. 101, p. 17727–17735.

Stern, R.J., and Dickinson, W.R., 2010, The Gulf of Mexico is a Jurassic backarc basin: Geosphere, v. 6, p. 739–754.

Turner, G., and Morton, A.C., 2007, The effects of burial diagenesis on detrital heavy mineral grain surface textures, *in* Mange, M.A., and Wright, D.T., eds., Heavy Minerals In Use: Developments in Sedimentology, v. 58, p. 393–412.

Venegas-Rodríguez, G., Barboza-Gudiño, J.R., and López-Doncel, R.A., 2009, Geocronología de circones detríticos en capas del Jurásico Inferior de las áreas de la Sierra de Catorce y El Alamito en el estado de San Luis Potosí: Revista Mexicana de Ciencias Geológicas, v. 26, p. 466–481.

Vermeesch, P., 2012, On the visualisation of detrital age distributions: Chemical Geology, v. 312–313, p. 190–194.

Walker, J.D., Geissman, J.W., Bowring, S.A., and Babcock, L.E., compilers, 2018, Geologic Time Scale v. 5.0: Geological Society of America, https://doi.org/10.1130/2018.CTS005R3C. ©2018 The Geological Society of America

Weber, B., Scherer, E.E., Martens, U.K., and Mezger, K., 2012, Where did the lower Paleozoic rocks of Yucatan come from? A U–Pb, Lu–Hf, and Sm–Nd isotope study: Chemical Geology, v. 312–313, p. 1–17.

Weltje, G.J., 2006, Ternary sandstone composition and provenance: an evaluation of the 'Dickinson model', in Buccianti, A., Mateu-Figueiras, G., and Pawlowsky-Glahn, V., eds., Compositional Data Analysis in the Geosciences: from Theory to Practice: Geological Society of London Special Publication, v. 264, p. 79–99.

Whitney, D.L., and Evans, B.W., 2010, Abbreviations for names of rock-forming minerals: American Mineralogist, v. 95, p. 185–187.

Winchester, J.A., and Floyd, P.A., 1977, Geochemical discrimination of different magma and their differentiation products using immobile trace elements: Chemical Geology, v. 20, p. 325–345.

Zimmermann, U., and Bahlburg, H., 2003, Provenance analysis and tectonic setting of the Ordovician clastic deposits in the southern Puna Basin, NW Argentinia: Sedimentology, v. 50, p. 1079–1104.

**Figure captions**

**Figure 1.** Map after Lawton and Molina-Garza (2014) illustrating the inferred trend of the Jurassic continental-margin arc through Mexico. The location of the geologic map shown in Figure 2 is indicated by the square. Abbreviations: AZ—Arizona; CHI—Chihuahua; COA—Coahuila; DUR—Durango; NL—Nuevo León; NM—New Mexico; SLP—San Luis Potosí; SON—Sonora; TMP—Tamaulipas; TX—Texas; ZAC—Zacatecas.

**Figure 2.** Detail of central and northeastern Mexico showing the location of the studied sections (La Ballena, Charcas and Real de Catorce) in the Mesa Central region (after Barboza-Gudiño et al., 2010).

**Figure 3.** Illustration of different stratigraphic units in the Sierra Madre Oriental and the Mesa Central region provided by different authors (modified from Barboza-Gudiño et al., 2010). The ages of stratigraphic boundaries are according to Gradstein et al. (2012).

**Figure 4.** Schematic lithostratigraphic columns for the three studied sections in the Mesa Central region in central Mexico, according to field mapping by the authors.

**Figure 5.** Thin section photomicrographs under plane-polarised light (left side) and under crossed polars (right side), respectively, of a selection of sandstone samples analyzed in this study. **(a, b)** Sample Cha B10, La Joya Formation. **(c, d)** Sample Cha B11, La Joya Formation. **(e, f)** Sample RdC C2, Zacatecas Formation. **(g, h)** Sample RdC C6a, Zacatecas Formation. The *scale bar* represents 1000 μm in all images. *Qm* – Monocrystalline quartz; *Qp* – Polycrystalline quartz; *Kfs* – K-feldspar; *Pl* – Plagioclase; *Lv* – Volcanic lithoclasts.

**Figure 6.** QFL diagram for sandstone classification (after Dott, 1964) and QFL diagram for interpretation of the provenance of sediments (after Weltje, 2006). *Q* – Total quartz (Qm+Qp); *F* – Total feldspar; *L* – Total lithic fragments.

**Figure 7.** Discrimination diagrams for revealing sediment recycling and provenance. For comparision, the volcanic rocks are also shown. **(a)** Diagram after McLennan et al. (1993). **(b)** Diagram after Floyd and Leveridge (1987). **(c)** Cr vs. Ni diagram. Values of Cr (>150 ppm) and Ni (>100 ppm) and a high correlation coefficient between Cr and Ni are diagnostic of ultramafic rocks in the source area (Garver et al., 1996; Meinhold et al., 2009). Upper continental crust (UCC) according to Rudnick and Gao (2003).

**Figure 8.** Relative abundance of detrital heavy minerals in the 63–125 μm fraction of the sandstone and volcanic rock samples from the Mesa Central region in central Mexico, expressed as frequency in %. Samples are ordered according to stratigraphy. *Pxn* – Pyroxene; *Amp* – Amphibole; *Ep* – Epidote; *Spn* – Sphene; *Grt* – Garnet; *Chl* – Chlorite; *Tur* – Tourmaline; *Rt* – Rutile; *Ant* – Anatase; *Zrn* – Zircon; *Ap* – Apatite.

**Figure 9.** Variation of heavy mineral index values and the ZTR values in sandstone and volcanic rocks samples from the Mesa Central region of central Mexico. Samples are ordered according to stratigraphy. ATi, RuZi and GZi were calculated following Morton and Hallsworth (1994, 1999). The whole-rock $SiO_2$ content is shown for comparison.

**Figure 10.** Cathodoluminescence images of representative zircon grains from samples analyzed in this study with location of the LA-ICP-MS analysis spot and corresponding $^{206}Pb/^{238}U$ age (±2-sigma) in Ma. The source formation for samples La BA3 and Cha B8 is La Joya Formation, for sample RdC C8 the Nazas Formation and for sample RdC C4 the Zacatecas Formation.

**Figure 11.** Kernel density estimation (KDE) and histograms for detrital zircons from lower Mesozoic sandstone samples of the Mesa Central region of central Mexico. Zircon populations of the four main potential source areas are shown with shaded bars. The open circles represent the age for each grain zircon. Only grains with 95 to 105% concordance are shown.

**Figure 12.** Conventional (Wetherill) concordia diagram showing detrital zircon U–Pb ages of the youngest age population in sample LaB A3. Note that zircon grain A3_19 ($^{206}Pb/^{238}U$ age = 149.9 ± 3.5 Ma) is not shown and was excluded from the concordia age calculation using the Isoplot Excel macro of Ludwig (2003).

**Figure 13.** Palaeogeographic map for the Middle Jurassic showing sediment transport paths from Oaxaquia (pink arrows), Pan-African rocks (green), Paleozoic of the Acatlan complex (orange), Permian-Triassic arc (red), Nazas arc (purple) and precambrian rocks of South America (lilac) towards central Mexico (modified from Ortega-Flores et al., 2014).

**Tables**

**Table 1.** Sample list and summary of the applied methods. Samples are ordered according to sampling locality. Note that the volcanic rocks are classified by whole-rock geochemistry using XRF. Sample Lab A2 was not analyzed by XRF.

**Table 2.** Petrographic data of thin sections. Samples are ordered according to stratigraphy.

**Table 3.** Illustration of the weighted average age of the youngest zircon age population and the youngest grain ages. The full set of isotopic data is in Tables S7–S13 (see Supplementary data).

**Supplementary data**

**Tables S4–S13**

Supplemental data are available online at xxxxx.

Table S4. Whole-rock geochemical data using XRF supplemented by LOI. Total iron is given as $FeO_t$. Samples are ordered according to stratigraphy.

Table S5. Relative abundance of opaque and non-opaque heavy minerals in the 63–125 μm fraction of the sandstones and two volcanic rock samples from the Mesa Central region in central Mexico, expressed as frequency in %. Samples are ordered according to stratigraphy.

Table S6. Relative abundance of non-opaque heavy minerals in the 63–125 μm fraction of the sandstones and two volcanic rock samples from the Mesa Central region in central Mexico, expressed as frequency in %. Samples are ordered according to stratigraphy. The provenance-senitive ratio parameters were calculated following Morton and Hallsworth (1994, 1999). The ZTR index is acoording to Hubert (1962).

Tables S7–13: Summary of U–Pb zircon results.

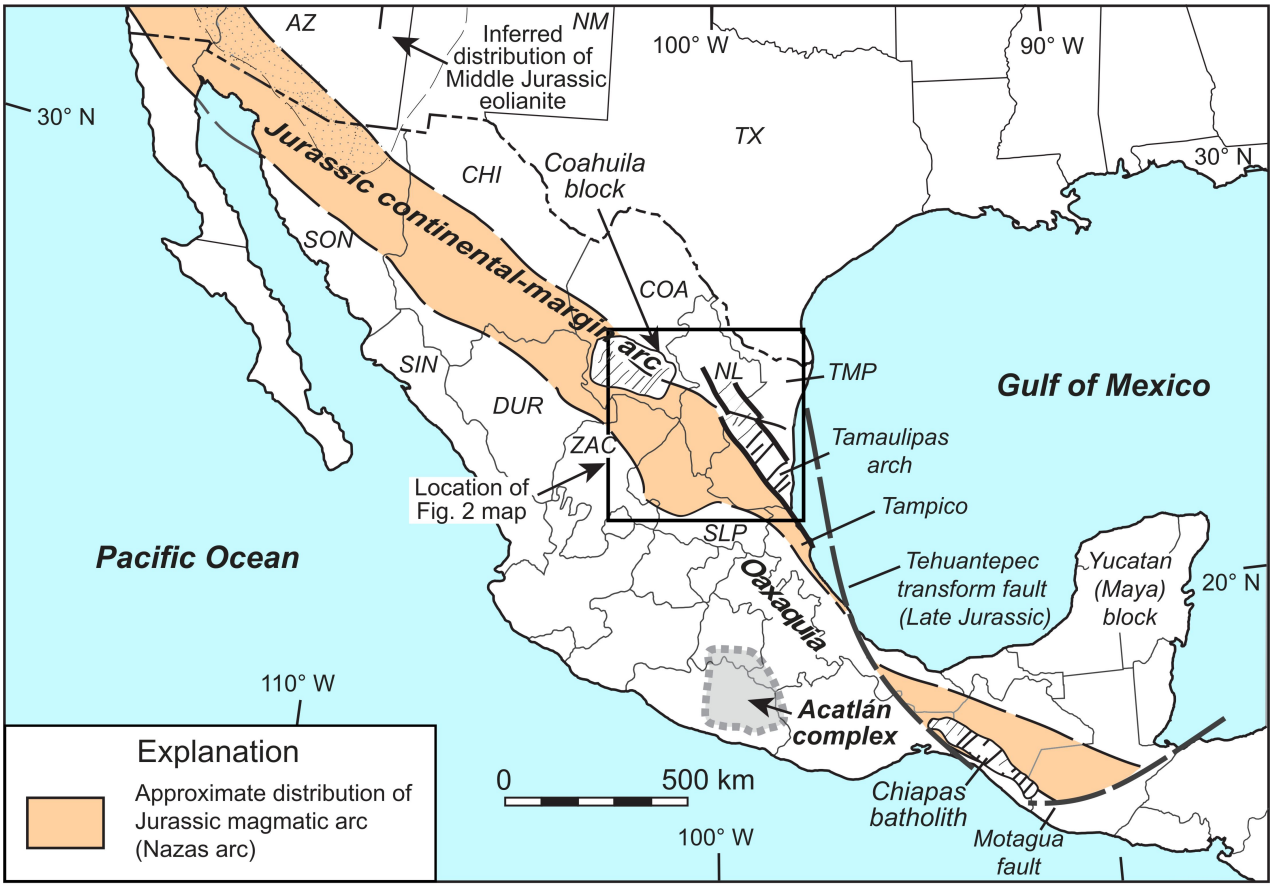
AZ
NM
Inferred distribution of Middle Jurassic eolianite
100° W
90° W
30° N
TX
CHI
Coahuila block
Jurassic continental-margin arc
SON
COA
SIN
NL
TMP
Gulf of Mexico
DUR
ZAC
Tamaulipas arch
Location of Fig. 2 map
Tampico
SLP
Pacific Ocean
Oaxaquia
Tehuantepec transform fault (Late Jurassic)
Yucatan (Maya) block
20° N
110° W
Acatlán complex
Explanation
Approximate distribution of Jurassic magmatic arc (Nazas arc)
0
500 km
Chiapas batholith
100° W
Motagua fault

Fig. 1

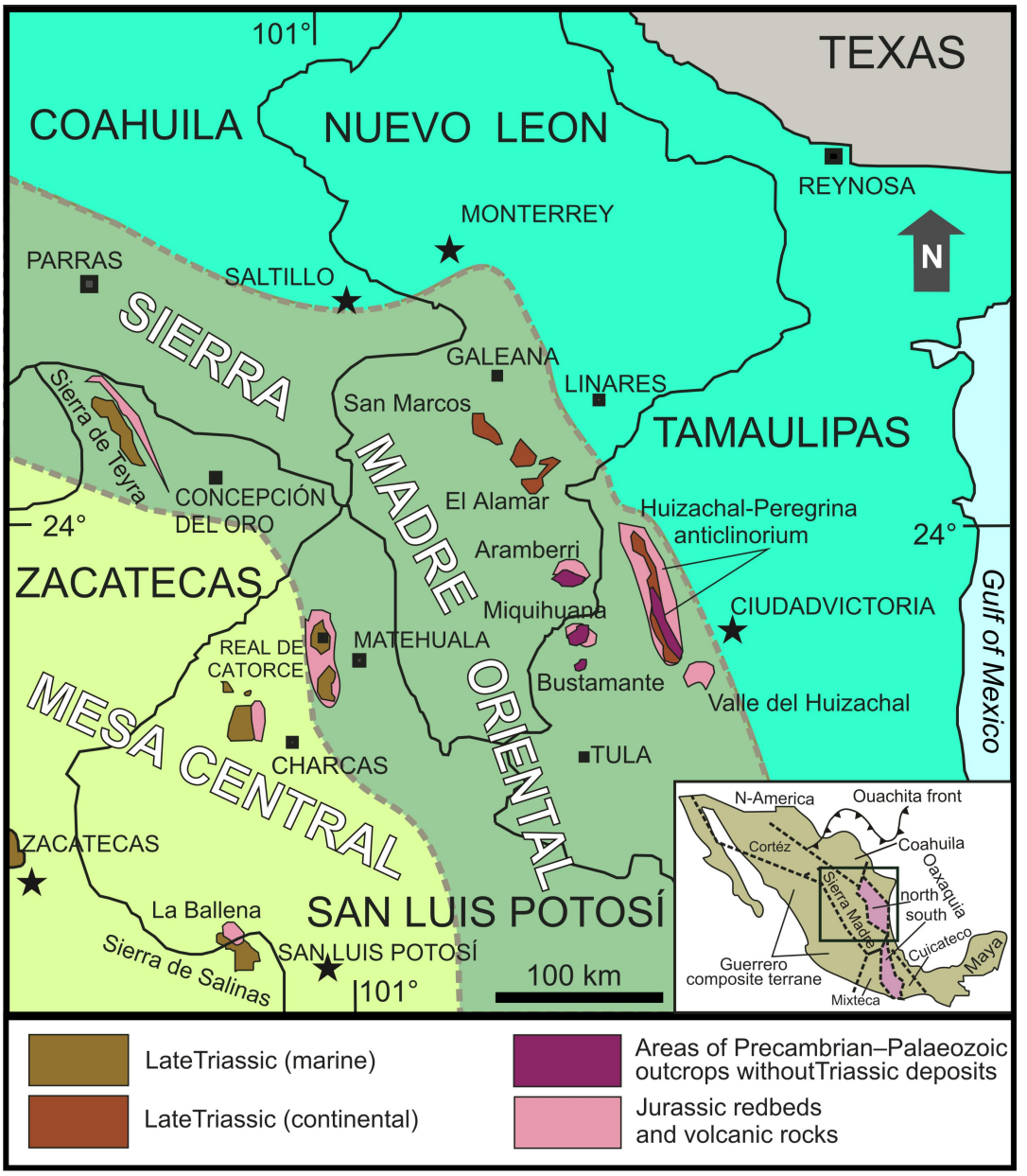
101°
TEXAS
COAHUILA
NUEVO LEON
REYNOSA
MONTERREY
N
PARRAS
SALTILLO
SIERRA
GALEANA
LINARES
San Marcos
Sierra de Teyra
TAMAULIPAS
MADRE ORIENTAL
CONCEPCIÓN DEL ORO
El Alamar
Huizachal-Peregrina anticlinorium
24°
24°
Aramberri
ZACATECAS
Miquihuana
CIUDADVICTORIA
Gulf of Mexico
REAL DE CATORCE
MATEHUALA
Bustamante
Valle del Huizachal
MESA CENTRAL
CHARCAS
TULA
ZACATECAS
La Ballena
SAN LUIS POTOSÍ
Sierra de Salinas
SAN LUIS POTOSÍ
101°
100 km
N-America
Ouachita front
Cortéz
Coahuila
Oaxaquia
Sierra Madre
north
south
Cuicateco
Maya
Guerrero composite terrane
Mixteca
LateTriassic (marine)
LateTriassic (continental)
Areas of Precambrian–Palaeozoic outcrops withoutTriassic deposits
Jurassic redbeds and volcanic rocks

Fig. 2

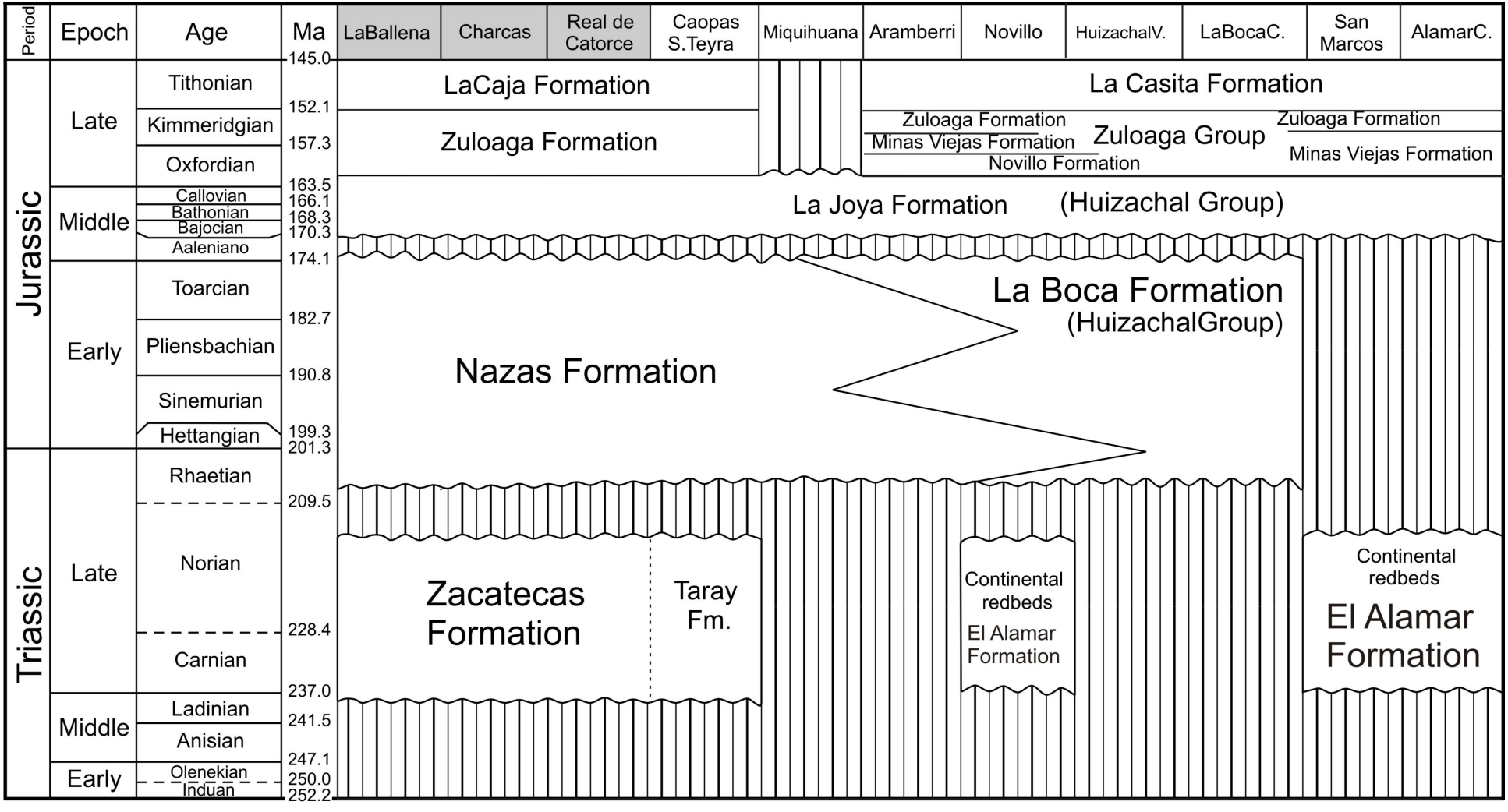
Period
Epoch
Age
Ma
LaBallena
Charcas
Real de Catorce
Caopas S.Teyra
Miquihuana
Aramberri
Novillo
HuizachalV.
LaBocaC.
San Marcos
AlamarC.
Jurassic
Triassic
Late
Middle
Early
Tithonian
Kimmeridgian
Oxfordian
Callovian
Bathonian
Bajocian
Aaleniano
Toarcian
Pliensbachian
Sinemurian
Hettangian
Rhaetian
Norian
Carnian
Ladinian
Anisian
Olenekian
Induan
145.0
152.1
157.3
163.5
166.1
168.3
170.3
174.1
182.7
190.8
199.3
201.3
209.5
228.4
237.0
241.5
247.1
250.0
252.2
LaCaja Formation
Zuloaga Formation
La Casita Formation
Zuloaga Formation
Minas Viejas Formation
Novillo Formation
Zuloaga Group
Zuloaga Formation
Minas Viejas Formation
La Joya Formation
(Huizachal Group)
La Boca Formation
(HuizachalGroup)
Nazas Formation
Zacatecas Formation
Taray Fm.
Continental redbeds
El Alamar Formation
Continental redbeds
El Alamar Formation

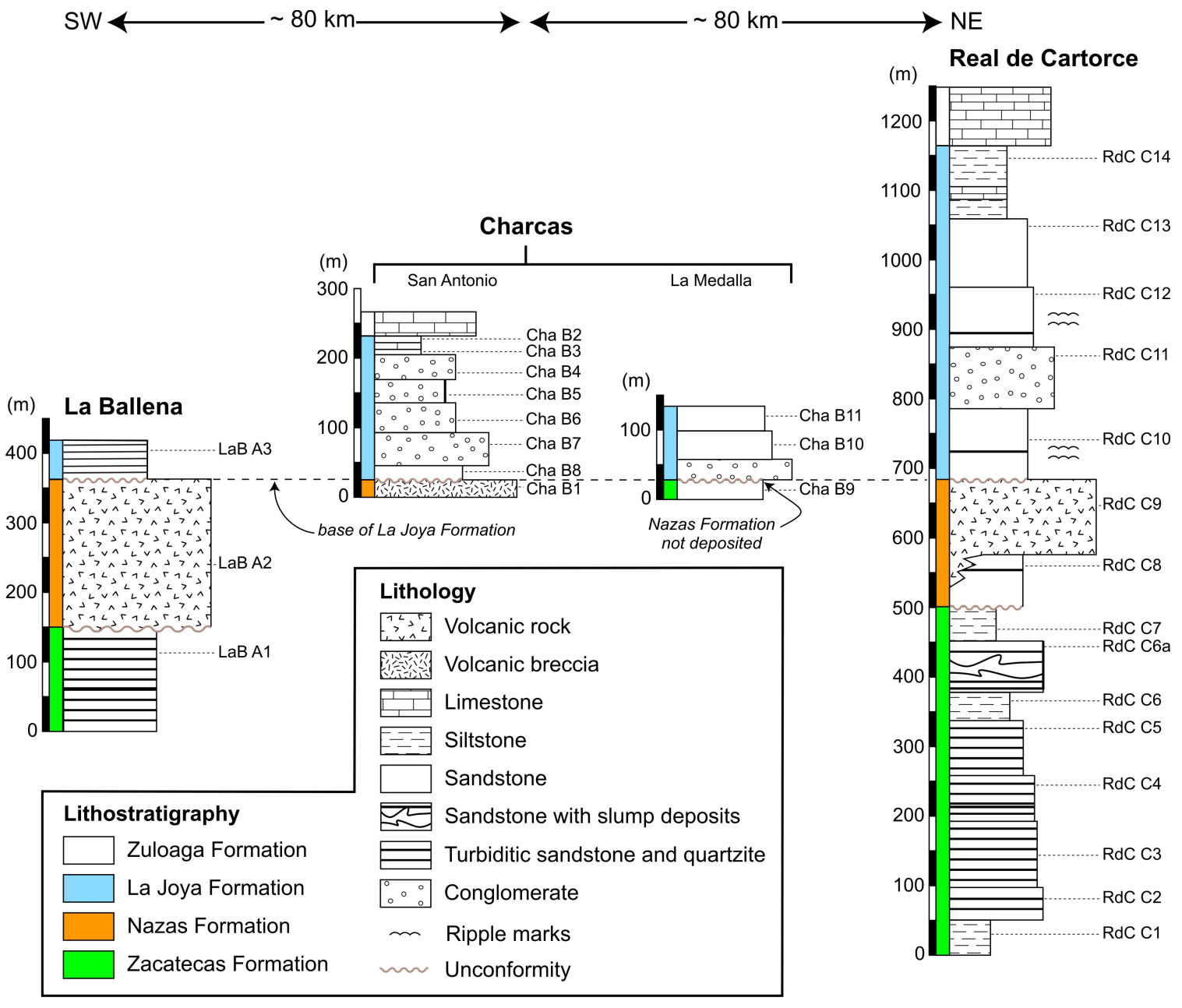
SW
~ 80 km
~ 80 km
NE
Real de Cartorce
(m)
1200
1100
1000
900
800
700
600
500
400
300
200
100
0
RdC C14
RdC C13
RdC C12
RdC C11
RdC C10
RdC C9
RdC C8
RdC C7
RdC C6a
RdC C6
RdC C5
RdC C4
RdC C3
RdC C2
RdC C1
Charcas
San Antonio
La Medalla
(m)
300
200
100
0
Cha B2
Cha B3
Cha B4
Cha B5
Cha B6
Cha B7
Cha B8
Cha B1
(m)
100
0
Cha B11
Cha B10
Cha B9
Nazas Formation
not deposited
base of La Joya Formation
La Ballena
(m)
400
300
200
100
0
LaB A3
LaB A2
LaB A1
Lithology
Volcanic rock
Volcanic breccia
Limestone
Siltstone
Sandstone
Sandstone with slump deposits
Turbiditic sandstone and quartzite
Conglomerate
Ripple marks
Unconformity
Lithostratigraphy
Zuloaga Formation
La Joya Formation
Nazas Formation
Zacatecas Formation

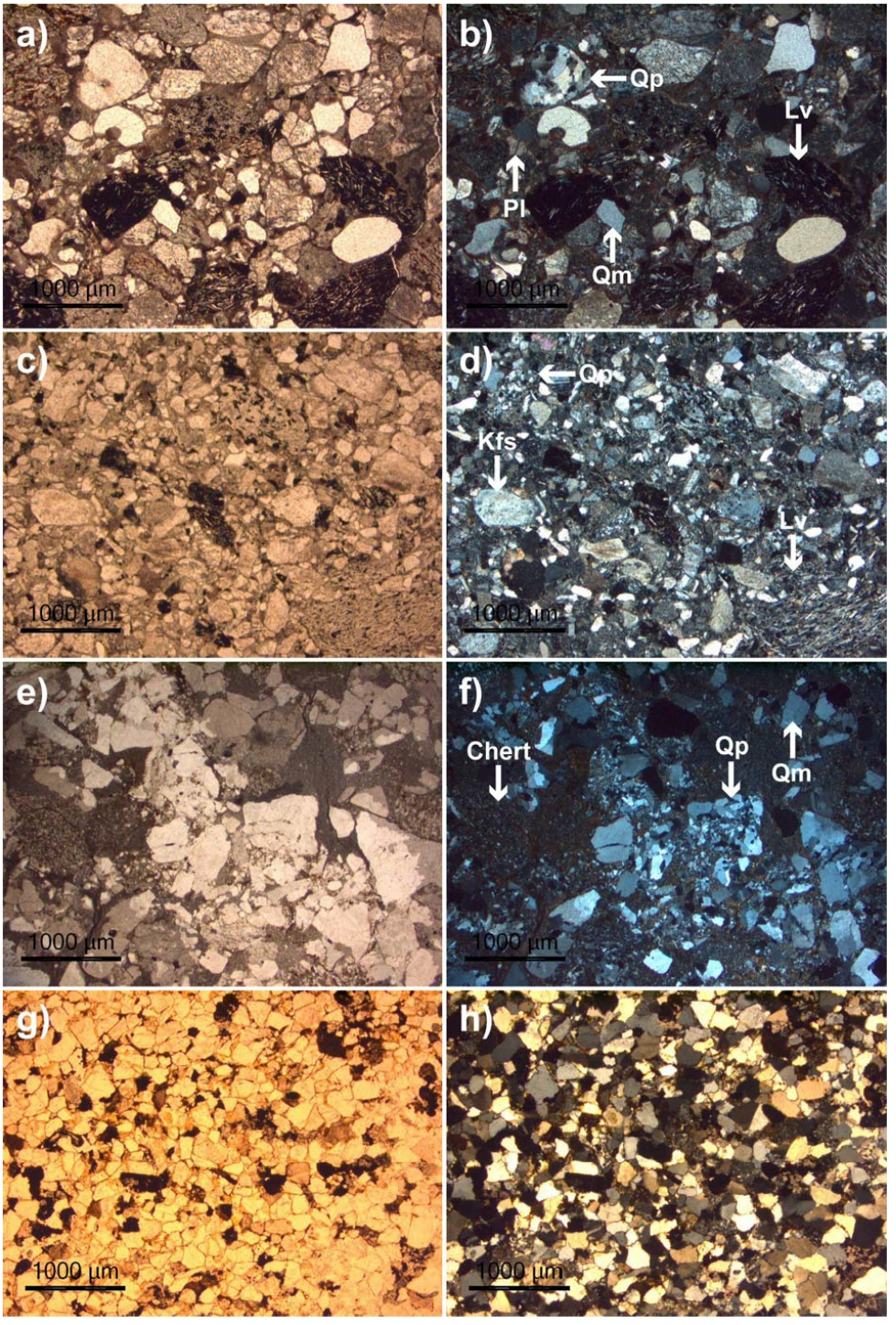
a)
1000 µm
b)
Qp
Lv
Pl
Qm
1000 µm
c)
1000 µm
d)
Qp
Kfs
Lv
1000 µm
e)
1000 µm
f)
Chert
Qp
Qm
1000 µm
g)
1000 µm
h)
1000 µm

Fig. 5

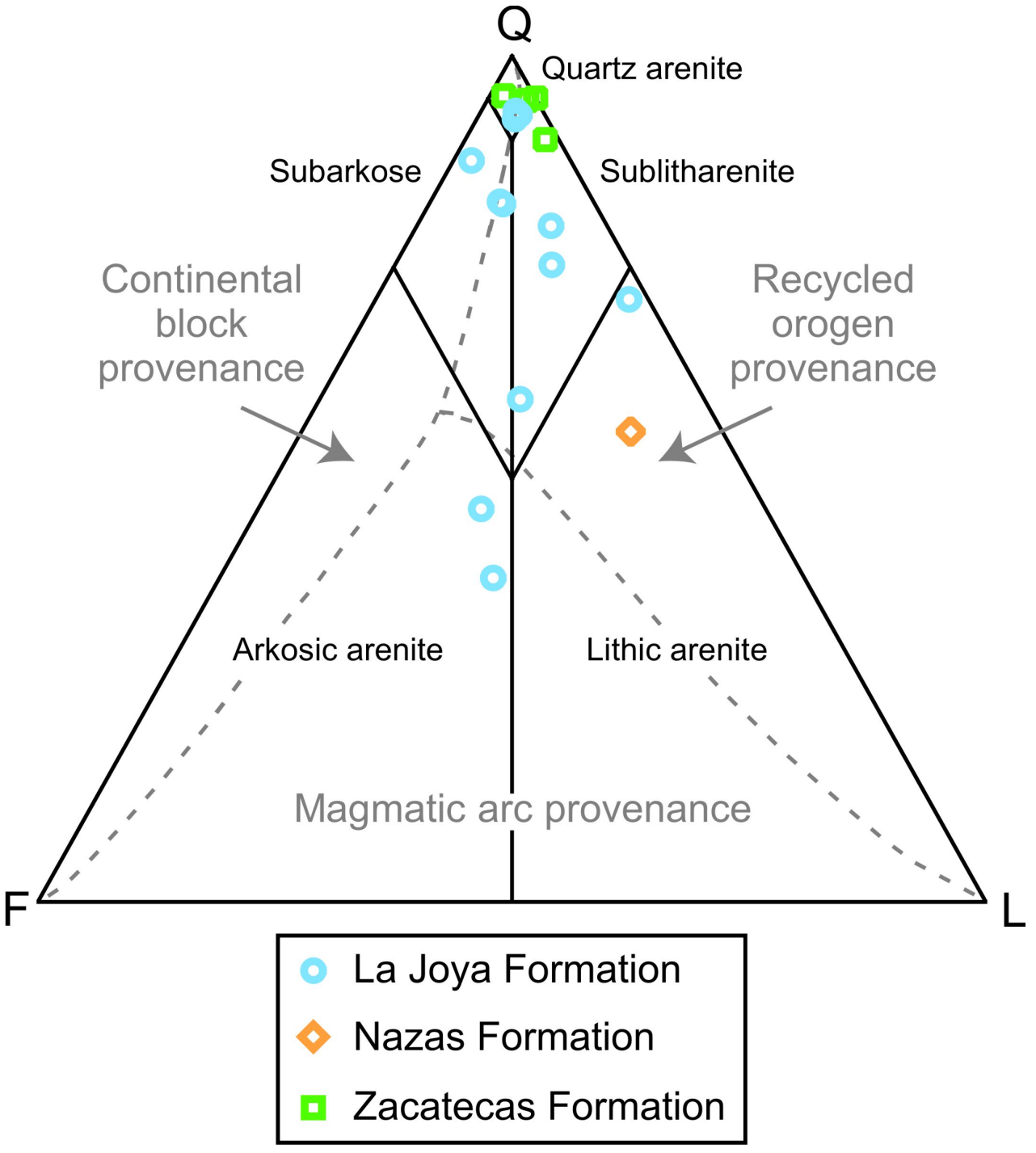
Q
Quartz arenite
Subarkose
Sublitharenite
Continental block provenance
Recycled orogen provenance
Arkosic arenite
Lithic arenite
Magmatic arc provenance
F
L
La Joya Formation
Nazas Formation
Zacatecas Formation

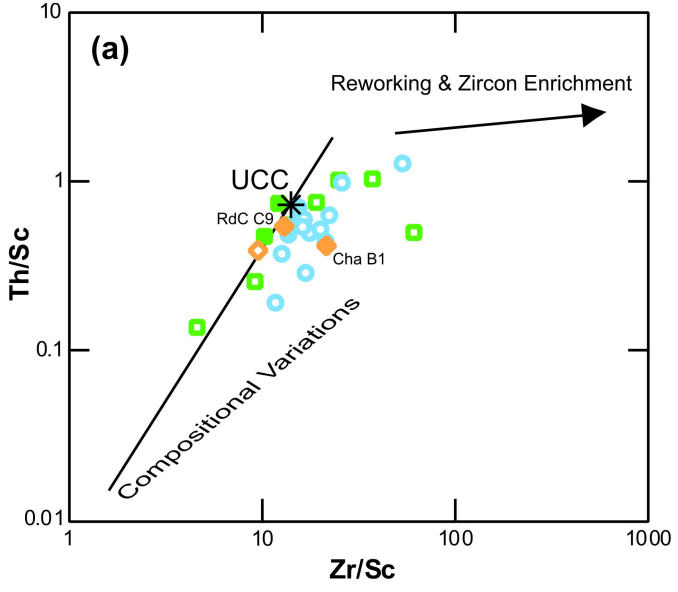
(a)
Reworking & Zircon Enrichment
UCC
RdC C9
Cha B1
Compositional Variations
Th/Sc
Zr/Sc
10
1
0.1
0.01
1
10
100
1000

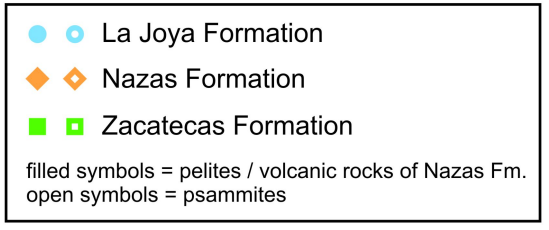
La Joya Formation
Nazas Formation
Zacatecas Formation
filled symbols = pelites / volcanic rocks of Nazas Fm.
open symbols = psammites

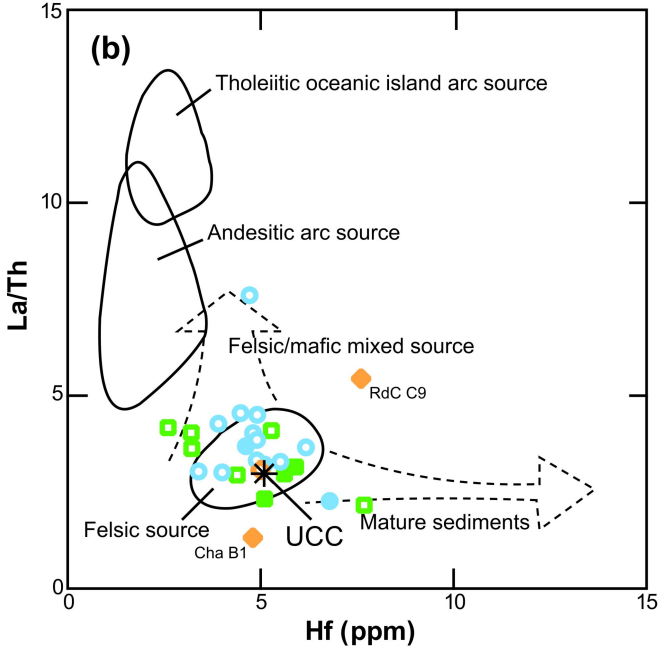
(b)
Tholeiitic oceanic island arc source
Andesitic arc source
Felsic/mafic mixed source
RdC C9
Felsic source
Cha B1
UCC
Mature sediments
La/Th
Hf (ppm)
15
10
5
0
0
5
10
15

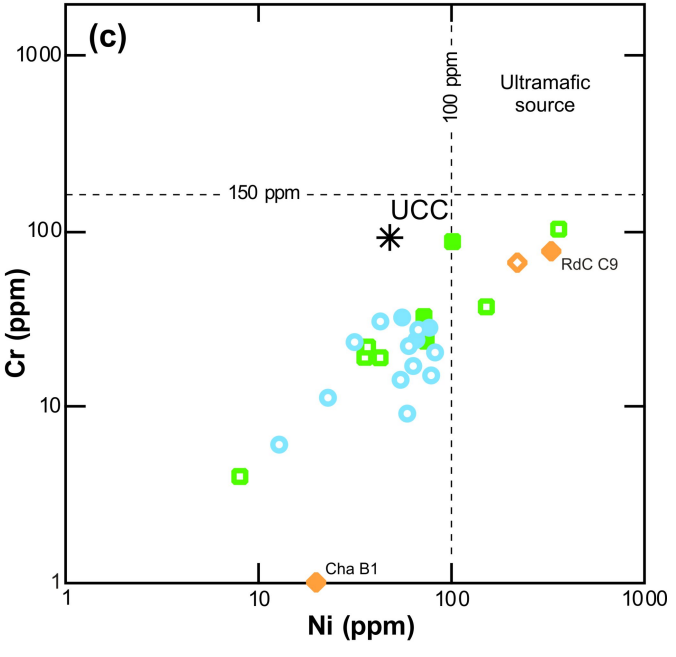
(c)
100 ppm
Ultramafic
source
150 ppm
UCC
RdC C9
Cha B1
Cr (ppm)
Ni (ppm)
1000
100
10
1
1
10
100
1000

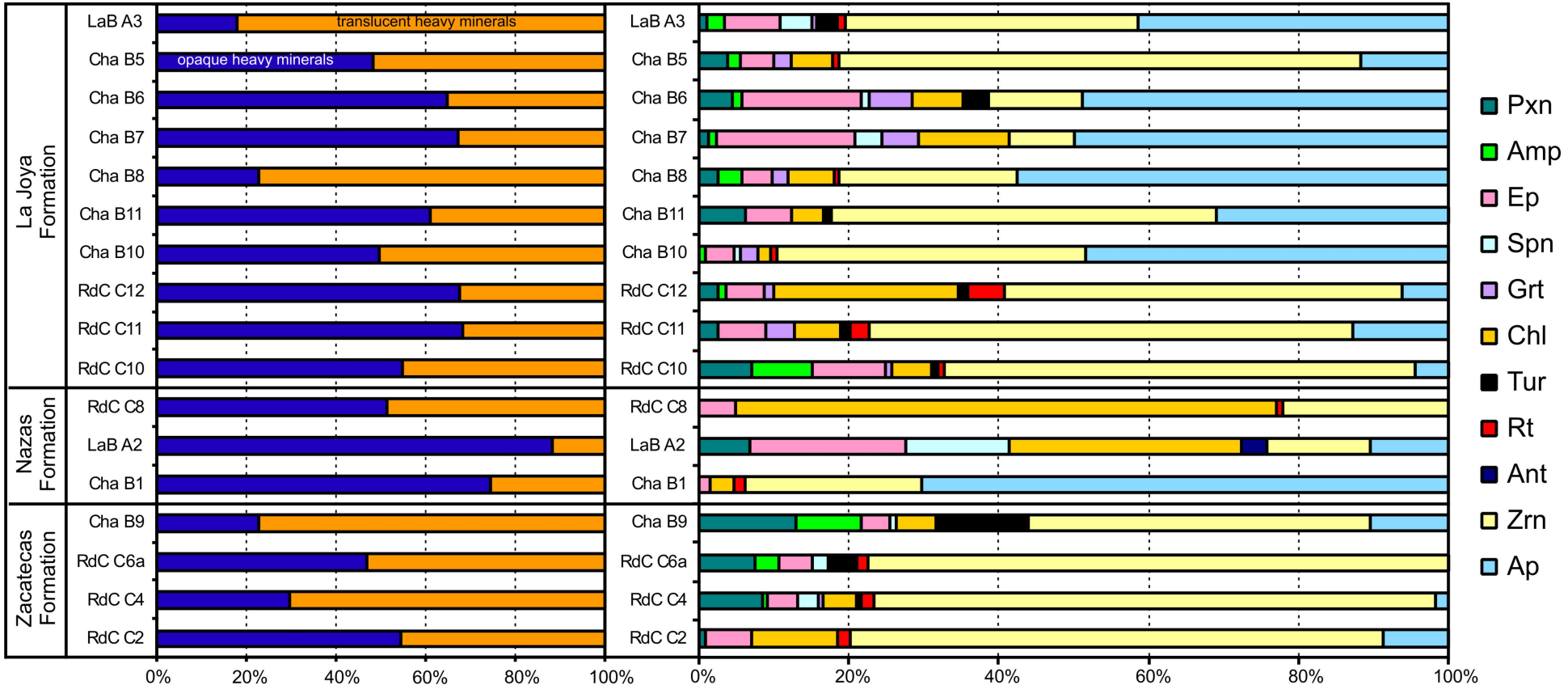
La Joya Formation
Nazas Formation
Zacatecas Formation
LaB A3
Cha B5
Cha B6
Cha B7
Cha B8
Cha B11
Cha B10
RdC C12
RdC C11
RdC C10
RdC C8
LaB A2
Cha B1
Cha B9
RdC C6a
RdC C4
RdC C2
translucent heavy minerals
opaque heavy minerals
0%
20%
40%
60%
80%
100%
Pxn
Amp
Ep
Spn
Grt
Chl
Tur
Rt
Ant
Zrn
Ap

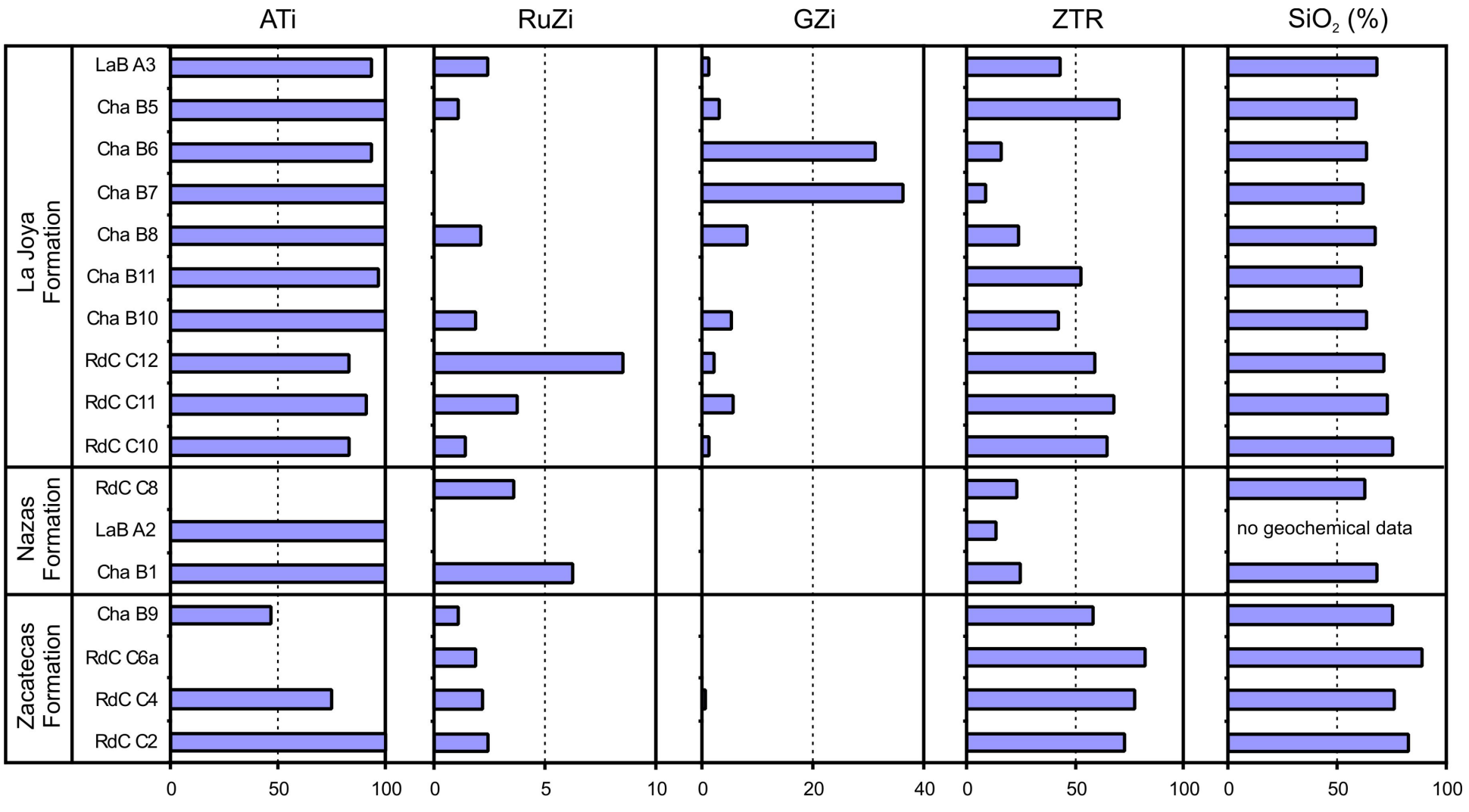
ATi
RuZi
GZi
ZTR
SiO2 (%)
La Joya Formation
Nazas Formation
Zacatecas Formation
LaB A3
Cha B5
Cha B6
Cha B7
Cha B8
Cha B11
Cha B10
RdC C12
RdC C11
RdC C10
RdC C8
LaB A2
Cha B1
Cha B9
RdC C6a
RdC C4
RdC C2
no geochemical data
0
50
100
0
5
10
0
20
40
0
50
100
0
50
100

Sample LaB A3, spot 7
158.6 ± 5.5 Ma

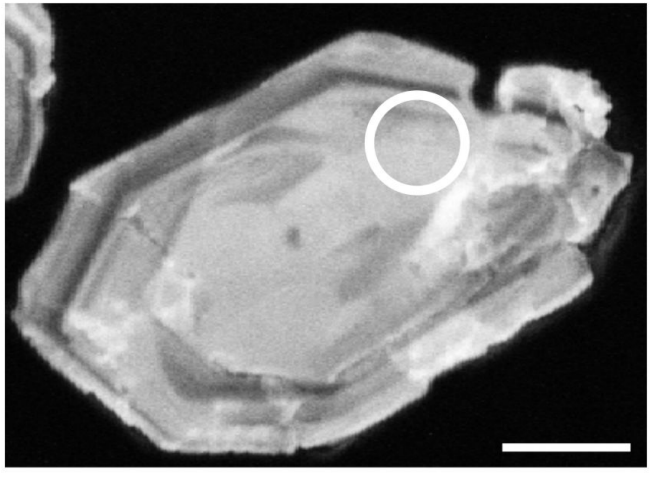

Scale bare = 30 μm

Sample Cha B8, spot 6
175.1 ± 2.5 Ma

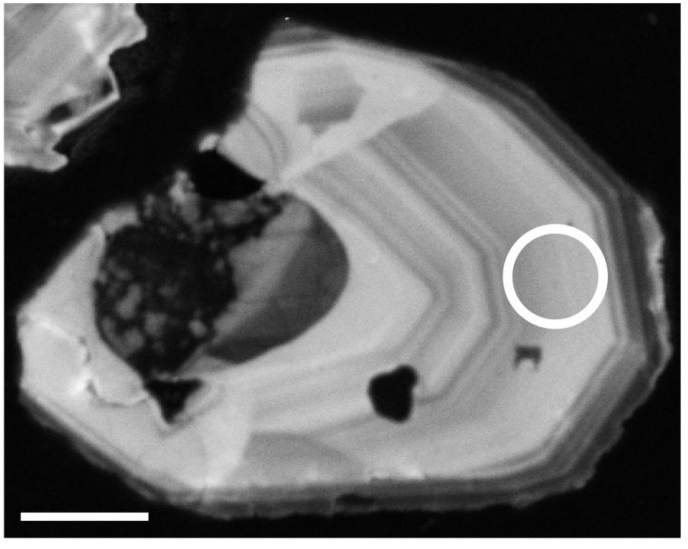

Sample RdC C8, spot 22
182.8 ± 8.7 Ma

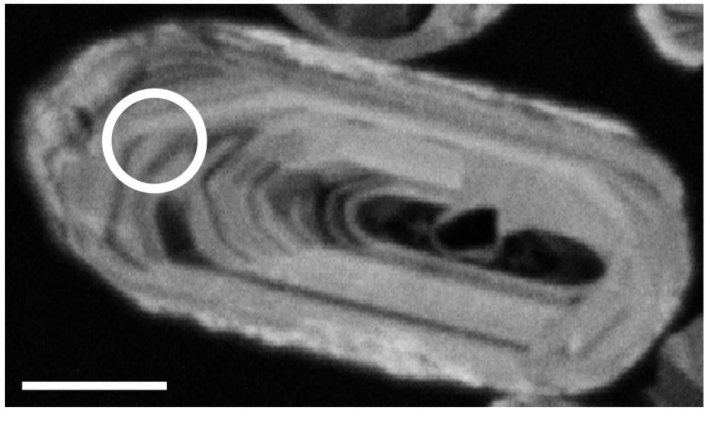

Sample RdC C4, spot 22
281.1 ± 3.2 Ma

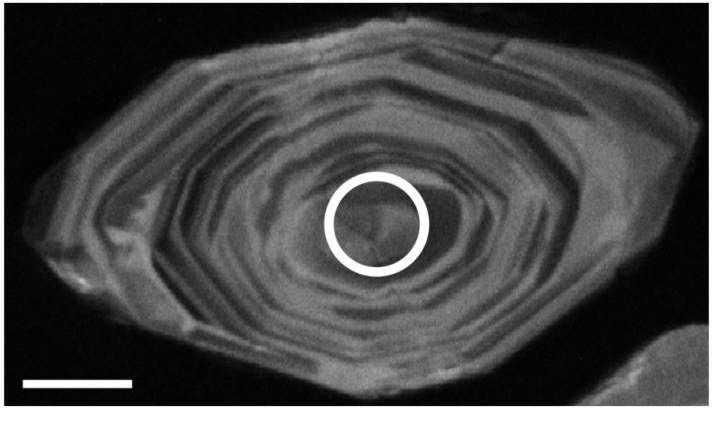

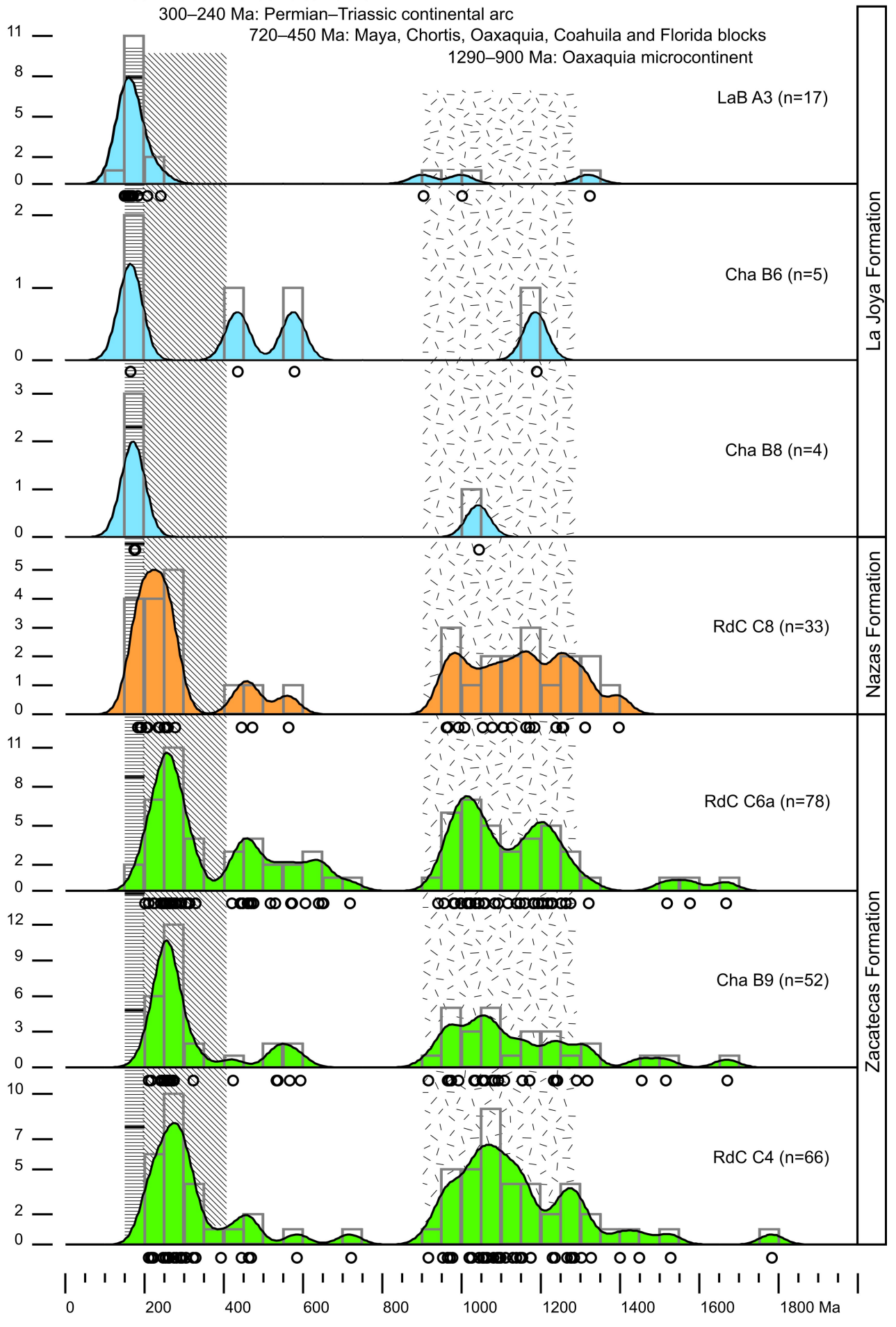
200–150 Ma: Nazas volcanic arc
300–240 Ma: Permian–Triassic continental arc
720–450 Ma: Maya, Chortis, Oaxaquia, Coahuila and Florida blocks
1290–900 Ma: Oaxaquia microcontinent
LaB A3 (n=17)
Cha B6 (n=5)
Cha B8 (n=4)
RdC C8 (n=33)
RdC C6a (n=78)
Cha B9 (n=52)
RdC C4 (n=66)
La Joya Formation
Nazas Formation
Zacatecas Formation
0
200
400
600
800
1000
1200
1400
1600
1800 Ma

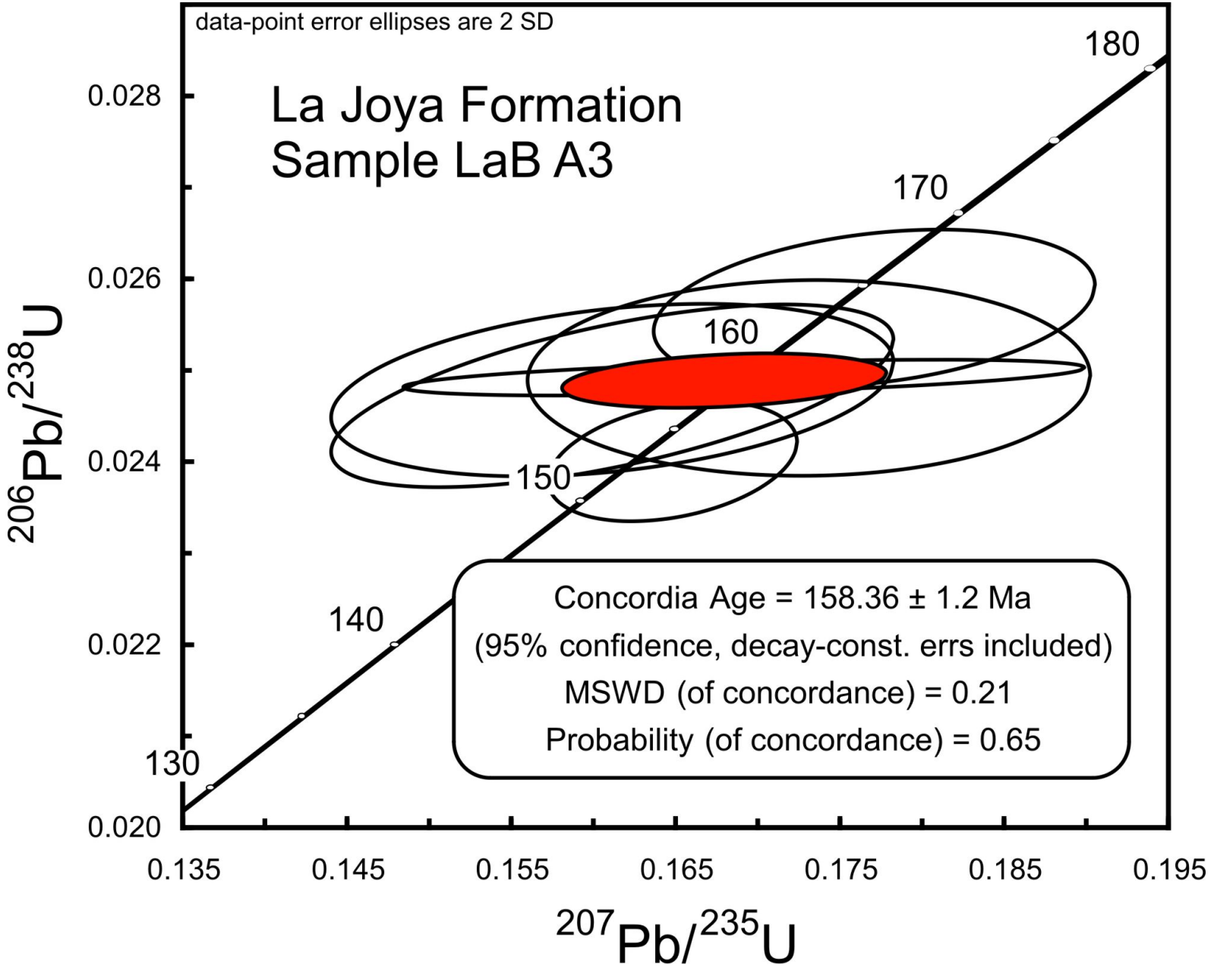
data-point error ellipses are 2 SD
La Joya Formation
Sample LaB A3
180
170
160
150
140
130
Concordia Age = 158.36 ± 1.2 Ma
(95% confidence, decay-const. errs included)
MSWD (of concordance) = 0.21
Probability (of concordance) = 0.65
0.028
0.026
0.024
0.022
0.020
206Pb/238U
0.135
0.145
0.155
0.165
0.175
0.185
0.195
207Pb/235U

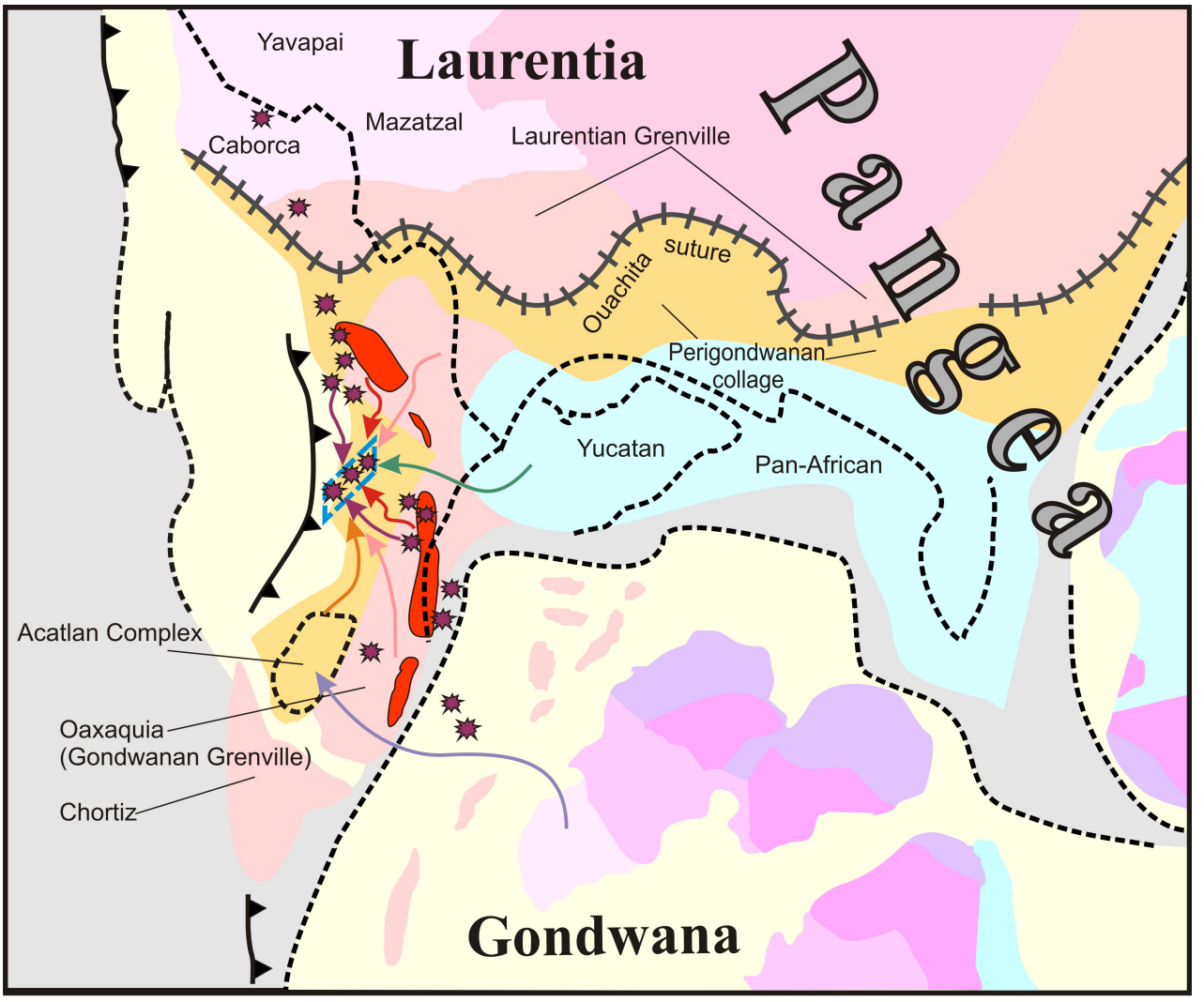


1.5-1.35 Ga

1.8-1.5 Ga

1.95-1.8 Ga

2.2-1.95 Ga

>2.3 Ga

Nazas arc
200-160 Ma

Permian-Triassic arc
300-240 Ma

1.2-1.1 Ga
0.48-0.36 Ga

0.68-0.54 Ga
0.42-0.41 Ga

1.3-1.0 Ga

Ancient subduction?

Geosuture

Study area

Late Paleozoic
and Mesozoic